iScience

CellPress
OPEN ACCESS

Article

Bumblebees land rapidly and robustly using a sophisticated modular flight control strategy

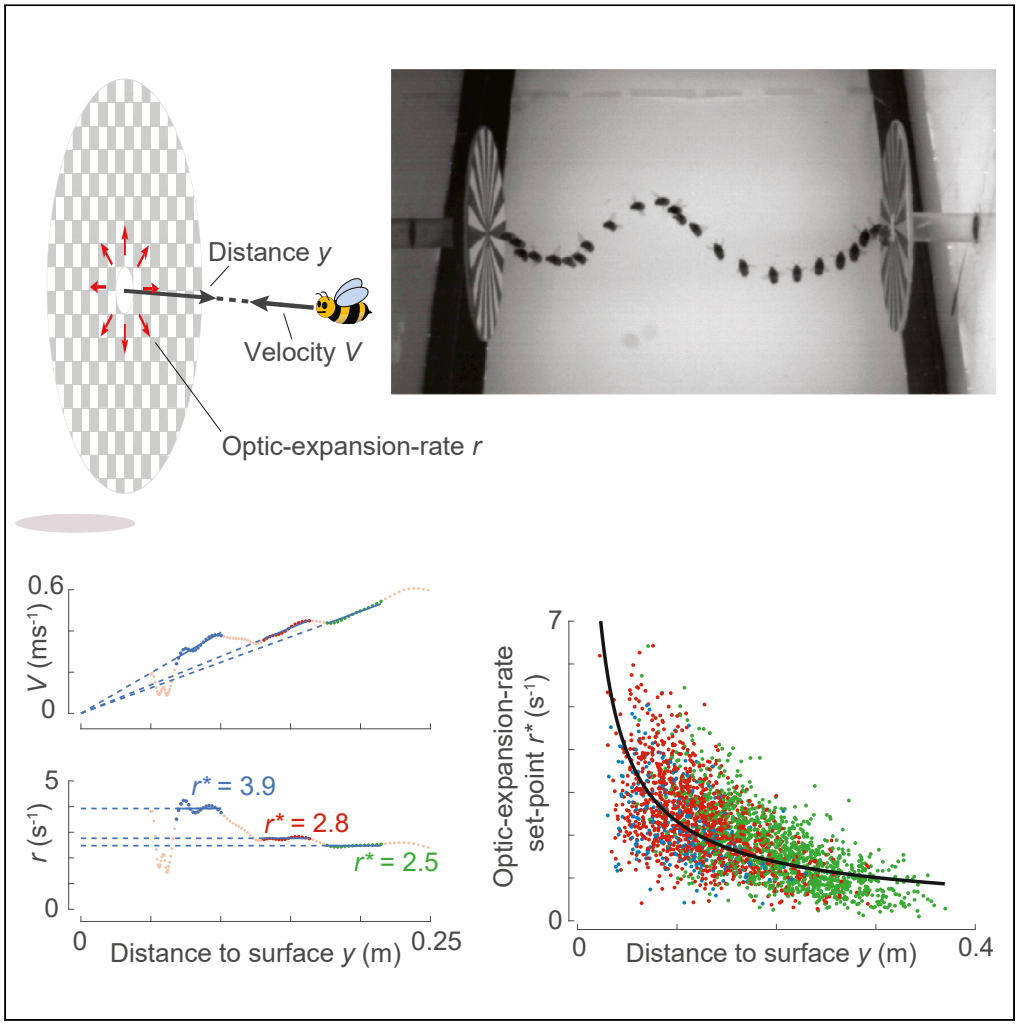

Pulkit Goyal, Antoine Cribellier, Guido C.H.E. de Croon, Martin J. Lankheet, Johan L. van Leeuwen, Remco P.M. Pieters, Florian T. Muijres

florian.muijres@wur.nl

Highlights

A custom-developed analysis method reveals how bumblebees control their landing

Landing bumblebees stepwise regulate the set point of optical expansion rate

Bumblebees land robustly in various challenging environmental conditions

Goyal et al., iScience 24, 102407
May 21, 2021
https://doi.org/10.1016/j.isci.2021.102407

iScience

CellPress
OPEN ACCESS

Article

Bumblebees land rapidly and robustly using a sophisticated modular flight control strategy

Pulkit Goyal,[1] Antoine Cribellier,[1] Guido C.H.E. de Croon,[2] Martin J. Lankheet,[1] Johan L. van Leeuwen,[1] Remco P.M. Pieters,[1] and Florian T. Muijres[1,3,*]

SUMMARY

When approaching a landing surface, many flying animals use visual feedback to control their landing. Here, we studied how foraging bumblebees (*Bombus terrestris*) use radial optic expansion cues to control in-flight decelerations during landing. By analyzing the flight dynamics of 4,672 landing maneuvers, we showed that landing bumblebees exhibit a series of deceleration bouts, unlike landing honeybees that continuously decelerate. During each bout, the bumblebee keeps its relative rate of optical expansion constant, and from one bout to the next, the bumblebee tends to shift to a higher, constant relative rate of expansion. This modular landing strategy is relatively fast compared to the strategy described for honeybees and results in approach dynamics that is strikingly similar to that of pigeons and hummingbirds. The here discovered modular landing strategy of bumblebees helps explaining why these important pollinators in nature and horticulture can forage effectively in challenging conditions; moreover, it has potential for bio-inspired landing strategies in flying robots.

INTRODUCTION

Landing is essential for all flying animals, and successful landings require precise control of flight momentum to perform soft touchdown. This is particularly relevant for foraging animals that use flight to routinely collect food. For example, bumblebees can perform more than 1000 landing maneuvers on flowers per hour (Heinrich, 1979). For each landing, the animal uses its sensory-motor system to control deceleration in such a manner that its flight speed reduces to near zero at touchdown, thereby maximizing landing success and minimizing the risk of impact injuries (Foster and Cartar, 2011).

Many flying animals, including birds and insects, use visual motion cues to control approach speed during landings (Lee et al., 1991; Lee et al., 1993; Van Breugel and Dickinson, 2012; Baird et al., 2013; Chang et al., 2016). The animal's motion relative to the landing surface generates a radially expanding optic flow field, in which various features in the image appear to move radially outward from the center of expansion (Gibson, 1955; Edwards and Ibbotson, 2007). Flying animals can use this rate of optical expansion along with the retinal size of an object (Wagner, 1982) or angular position of features in the visual field (Baird et al., 2013) to compute the "relative rate of expansion (r)" or its inverse, the instantaneous "time to contact" ($\tau = 1/r$, referred to as parameter *tau* in literature) (Lee, 1976; Sun and Frost, 1998; Lee et al., 2009; Balebail et al., 2019). The relative rate of expansion provides information about the ego-motion of the animal and equals the ratio between approach speed V and distance from the landing surface y ($r = V/y$); instantaneous time-to-contact equals the time until contact with the landing surface, should the animal continue to fly at its current flight speed ($\tau = y/V$). The animals can use this relative rate of expansion (or time to contact) to gradually reduce their flight speed when approaching the landing surface and touch down at near-zero speed (Lee et al., 1991; Lee et al., 1993, 2009; Baird et al., 2013).

Birds and insects decelerate during landing in different ways (Figure 1). Honeybees (*Apis mellifera ligustica*) have been shown to approach a landing surface (up until ~7 cm distance from the surface) by keeping the relative rate of expansion constant at a particular set point (Baird et al., 2013). By doing so, their approach speed decreases linearly with distance to the landing surface (Figure 1B). Fruit flies (*Drosophila melanogaster*) and bumblebees (*Bombus impatiens*) have been suggested to use similar strategies (Van Breugel and Dickinson, 2012; Baird

[1]Experimental Zoology Group, Wageningen University and Research, 6708 WD Wageningen, the Netherlands

[2]Control and Simulation, Faculty of Aerospace Engineering, Delft University of Technology, 2629 HS Delft, the Netherlands

[3]Lead contact

*Correspondence: florian.muijres@wur.nl

https://doi.org/10.1016/j.isci.2021.102407

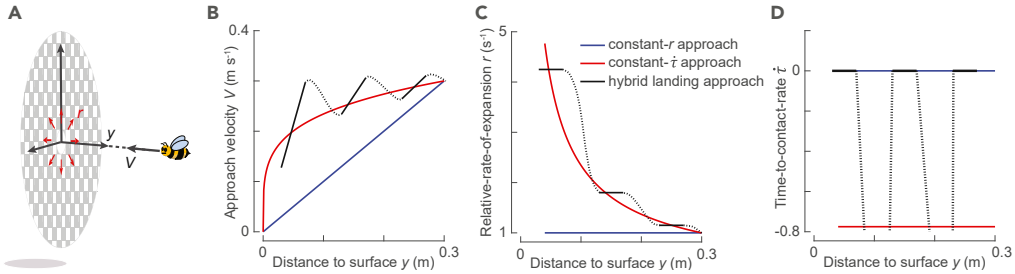

Figure 1. Illustration of landing strategies described in honeybees (blue) (Baird et al., 2013), birds (red) (Lee et al., 1991; Lee et al., 1993), and bumblebees as observed in this study (black).

(A) An animal that approaches a vertical landing platform along its axial direction experiences a relative optical expansion rate r as symbolized by the red arrows. At time t, the animal is at distance y from the object, has an approach flight velocity V, experiences a relative rate of expansion of $r = V/y$, and has an instantaneous time-to-contact $\tau = y/V$.

(B–D) The variation with distance from the landing surface of (B) approach velocity V, (C) relative rate of expansion r, and (D) time-to-contact rate ($\dot{\tau} = d\tau/dt$) for the constant-r landing approach observed in honeybees (blue) (Baird et al., 2013), the constant-$\dot{\tau}$ landing approach of birds (red) (Lee et al., 1991; Lee et al., 1993), and the here-observed hybrid landing approach of bumblebees (black). The hybrid landing approach consists of constant-r segments (solid lines), separated by transition phases (dotted curves). All results, and particularly the transition phases, are of idealized cases. Because birds and insects differ in size, there are large differences in distances and velocities between these landing strategies. For comparative purposes, we here show idealized versions of the three landing strategies with speeds and distances typical for bumblebees and honeybees, as all landings start at 0.3 m distance from the landing surface with an approach velocity of 0.3 m s^{-1}.

et al., 2013; Chang et al., 2016). Pigeons (*Columba livia*) and hummingbirds (*Colibri coruscans*), on the other hand, approach a landing surface by keeping the derivative of instantaneous time to contact constant (Figures 1B–1D, at a negative value as per sign convention in Figure 1A) (Lee et al., 1991; Lee et al., 1993). This derivative of "time to contact" ($\dot{\tau}$) is hereafter referred to as "time-to-contact rate" and defines how fast the animal decreases its time to contact, or increases its relative rate of expansion, during the landing maneuver (Figure 1C). Compared to honeybees, the avian landing strategy results in higher approach flight speeds, and hence faster landings (Figure 1B). From here on, we refer to the avian landing strategy as the constant-$\dot{\tau}$ strategy and the honeybee landing strategy as the constant-r strategy. Note that the constant-r strategy is a special case of the constant-$\dot{\tau}$ strategy whereby $\dot{\tau}$ is maintained at a value of zero ($\dot{\tau} = 0$).

Here, we study the landing maneuver dynamics of bumblebees (*Bombus terrestris*). Bumblebees are important pollinators in both nature and horticulture (Fontaine et al., 2006; Velthuis and van Doorn, 2006; Joar Hegland and Totland, 2008) owing to their ability to forage in a wide range of environmental conditions including relatively low temperatures (Corbet et al., 1993) and limited light conditions such as during twilight hours (Reber et al., 2015, 2016). Moreover, foraging bumblebees are efficient pollinators as they are able to visit more than 1000 flowers per hour (Heinrich, 1979). During such fast foraging actions, bumblebees tend to rapidly move from flower to flower in a single flower patch, followed by longer distance flights between patches. As a result, the average distance traveled between flowers in a fresh clover field is approximately 0.33 m (Heinrich, 1979).

To reproduce these foraging conditions, we trained bumblebees to routinely fly back and forth between two vertical landing platforms, one connected to their colony and the other to a food source (Figures 2A and 2B). We placed the landing platforms 0.34 m apart, which is similar to an average distance of 0.33 m traveled by bumblebees between landings when foraging on a fresh flower patch (Heinrich, 1979). The setup was placed in a large flight arena (Figures 2A and 2B), allowing the bumblebees to also exhibit the larger distance flights that resemble those between flower patches (Heinrich, 1979).

Using machine vision techniques, we then tracked 10,005 landing maneuvers of bumblebees. This data set consists of 2792 landings performed directly after taking off from the opposite platform or the ground, and 7213 landings following free flight. Moreover, to test how environmental conditions affect these landings, we varied the light intensity in three steps from twilight to sunrise conditions, and used two landing platforms with relatively low and high optical expansion information (Figure 2C).

We used two approaches to analyze the temporal deceleration dynamics of the landings. First, we analyzed how the average of multiple landing approaches varied among treatments (light condition and landing platform type)

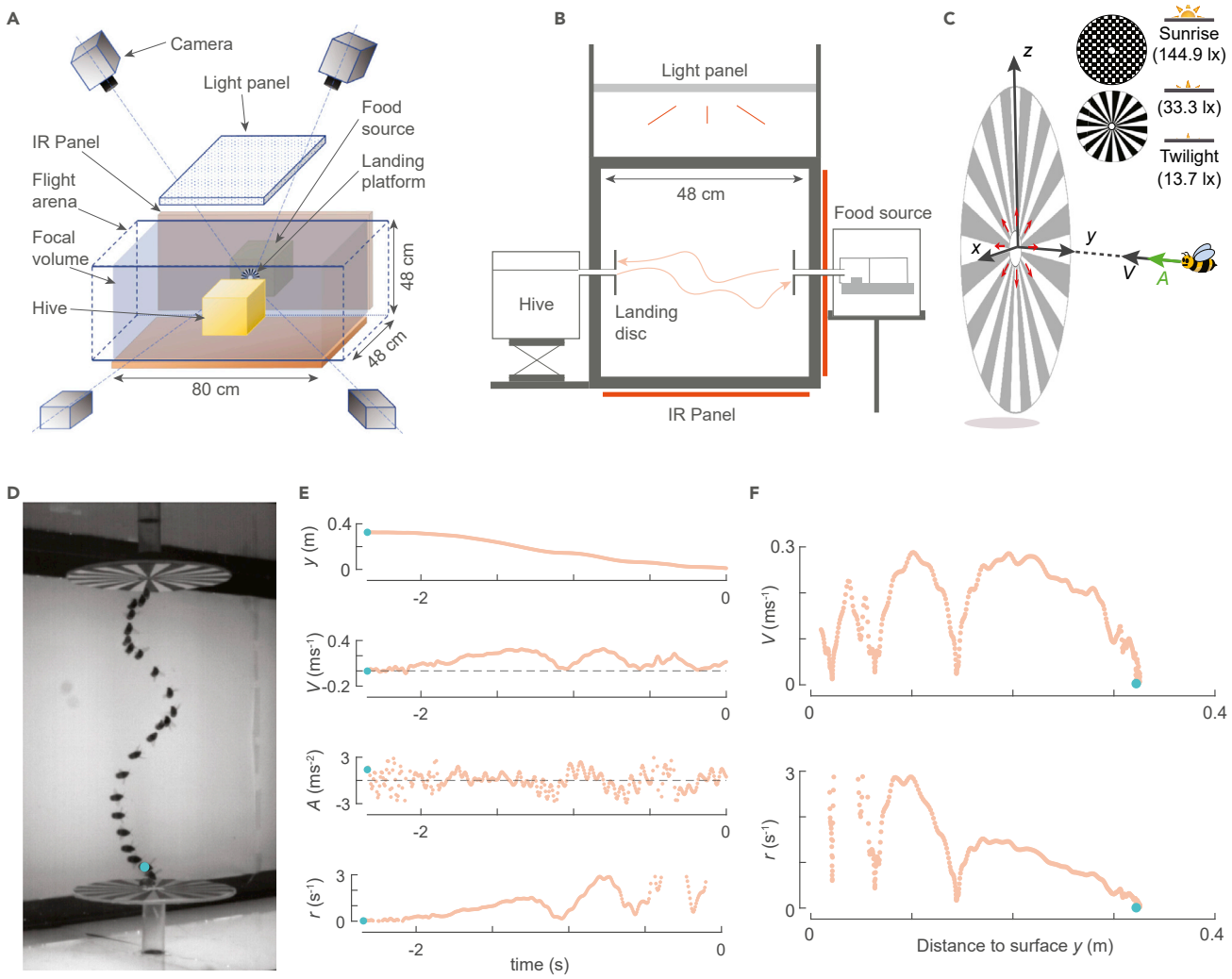

Figure 2. Experimental setup, definitions of the landing kinematics parameters, and temporal dynamics of a typical landing maneuver.

(A and B) The experimental setup consists of a flight arena with a four-camera high-speed videography system for tracking flying bumblebees, two vertical landing platforms connected to a hive and food source (outside the arena), and a LED light panel for varying the light conditions.

(C) The landing kinematics are described in a Cartesian coordinate system with its origin at the center of the landing platform, the *z* axis vertically up, and the *y* axis aligned along the axis of the disc and pointing into the flight arena. For each landing, we determined the temporal dynamics of approach distance *y*, velocity $V = -v_y$, and acceleration $A = -a_y$ along the *y* axis. The different landing patterns and light conditions used in this study are also shown.

(D–F) Flight dynamics of a bumblebee taking off and landing on a spoke landing platform; in all panels, the blue circle denotes the start of the flight sequence. (D) Photomontage from a downward-facing camera of the landing maneuver, at a time interval of ~0.1 s. (E) Temporal dynamics of the kinematics parameters (*y*, *V*, *A*) and the optical relative rate of expansion $r = V/y$, where time $t = 0$ s at touchdown. (F) The variation of *V* and *r* with perpendicular distance from the platform *y*.

and type of landing maneuvers (landing after takeoff and from free flight). This analysis strategy is similar to the one used previously to study the landing dynamics of bumblebees (*B. impatiens*) and honeybees (Baird et al., 2013; Chang et al., 2016). Second, we analyzed how the flight dynamics of individual landing maneuvers vary among the treatments and between landings after takeoff and from free flight. Hereafter, we refer to the former and the latter as the *average-per-treatment* and *per-track* analysis methods, respectively.

Our average-per-treatment analysis provides similar results as reported previously (Baird et al., 2013; Chang et al., 2016), showing that, on average, landing bumblebees decelerate linearly with reducing distance, in all tested conditions. This suggests that bumblebees use a constant-*r* landing strategy during both landings after takeoff and from free flight. In contrast, our per-track analysis shows that "individual bumblebees" do not do so, as they exhibit short intervals of deceleration at different set points of the relative rate of

expansion (Figure 1). During each set point, bumblebees keep their relative rate of expansion constant, and they increase their set point value as they reach closer to the surface. In fact, this increase in set points of relative rate of expansion with decreasing distance from the landing surface is governed on an average by a constant-$\dot{\tau}$ law, with $\dot{\tau}$ values similar to those of birds. Thus, on average, landing bumblebees approximate the landing strategies of birds by adjusting their constant-r set point in discrete steps as they approach the landing surface. Hence, this modular landing strategy of bumblebees can best be characterized as a hybrid between the constant-r and constant-$\dot{\tau}$ strategies described for honeybees and birds, respectively.

RESULTS

We trained a hive of bumblebees (*B. terrestris*) to forage for food in a flight arena equipped with a real-time automatic machine-vision-based three-dimensional insect tracking system (Straw et al., 2011) (Figure 2A). We placed a food source and hive on either side of the flight arena and connected them to two vertical landing platforms (0.18 m diameter). To collect food, the foraging bumblebees flew between the landing platforms and walked through the small aperture (0.02 m diameter) in the middle of the platform to access either the hive or the food source (Figure 2B).

During the experiments, we used landing platforms with either checkerboard or spoke patterns, as they provide a high and low amount of optical expansion flow information, respectively (Figure 2C). In addition, we varied the light intensity in the setup in three levels ranging from twilight to sunrise, referred to as low (13.7 lx), medium (33.3 lx), and high (144.9 lx) light conditions. Bumblebees continued to forage in all light conditions, allowing us to test how the landing strategy varied throughout the natural variation of challenging light conditions experienced by foraging bumblebees (Figure 2C). Light and platform conditions were systematically varied such that all combinations were tested (Table S1).

We placed the two landing platforms 0.34 m apart from each other, such that it resembles the 0.33 m average distance traveled between flowers by bumblebees foraging in a fresh clover patch (Heinrich, 1979). The flight arena (3 × 0.48 × 0.48 m; length × width × height) was large enough to capture not only landings directly after takeoff from the other platform but also landings from free flight (Figure S1). These landings represent those exhibited by bumblebees when traveling between flower patches or when traveling between the hive and foraging site.

We used the insect tracking system to determine the three-dimensional spatial-temporal dynamics of body location in 10,005 flight maneuvers of bumblebees approaching the landing platforms. Out of 10,005 landing approaches, 2792 landings followed after a takeoff from the ground or the opposite platform (Figures 2D–2F, Video S1) and 7213 landings occurred after free flight (Figures 3A and 3B). Irrespective of how bumblebees initiated their landing, most approach flights consisted of both acceleration and deceleration phases (Figure 2E). We hereafter focused only on the deceleration phases as we aimed to find out how bumblebees slowed down during their landing maneuver. For the landings following takeoff, the flight speed at the start of the landing maneuver was U_{start} = 0.11 [0.04, 0.24] m/s (median [first quartile, third quartile], n = 2792 landings), and for landings following free flight, this was U_{start} = 0.34 [0.21, 0.49] m/s (n = 7213 landings) (Figure S2). The free flight landings were thus initiated at flight speeds similar to those observed in previous bumblebee studies and sometimes even surpassed them (Reber et al., 2015; Chang et al., 2016).

The average flight kinematics of all recorded landing maneuvers

For each landing approach, we calculated the temporal dynamics of the following state variables (Figures 2D–2F): 3D position ($x(t)$, $y(t)$, $z(t)$), approach velocity ($V(t) = -dy(t)/dt$) and approach acceleration ($A(t) = -d^2y(t)/dt^2$) perpendicular to the landing platform, and the relative rate of expansion that a bumblebee experiences due to its motion perpendicular to the landing platform ($r(t) = V(t)/y(t)$).

On average, bumblebees performed the landing maneuver in a direction perpendicular to the platform (Figures 3A and 3B). During their mean landing maneuver, they advanced toward the platform by first gradually increasing their approach velocity (V), followed by a deceleration phase during which they decreased their approach velocity (0.04 m $\leq y \leq$ 0.11 m). As previously observed in honeybees (Baird et al., 2013) and suggested for bumblebees (*B. impatiens*) (Chang et al., 2016), the average decelerating bumblebee decreased its approach velocity approximately linearly with distance, thus keeping the relative rate of expansion nearly constant at a set point r^* (Figure 3C).

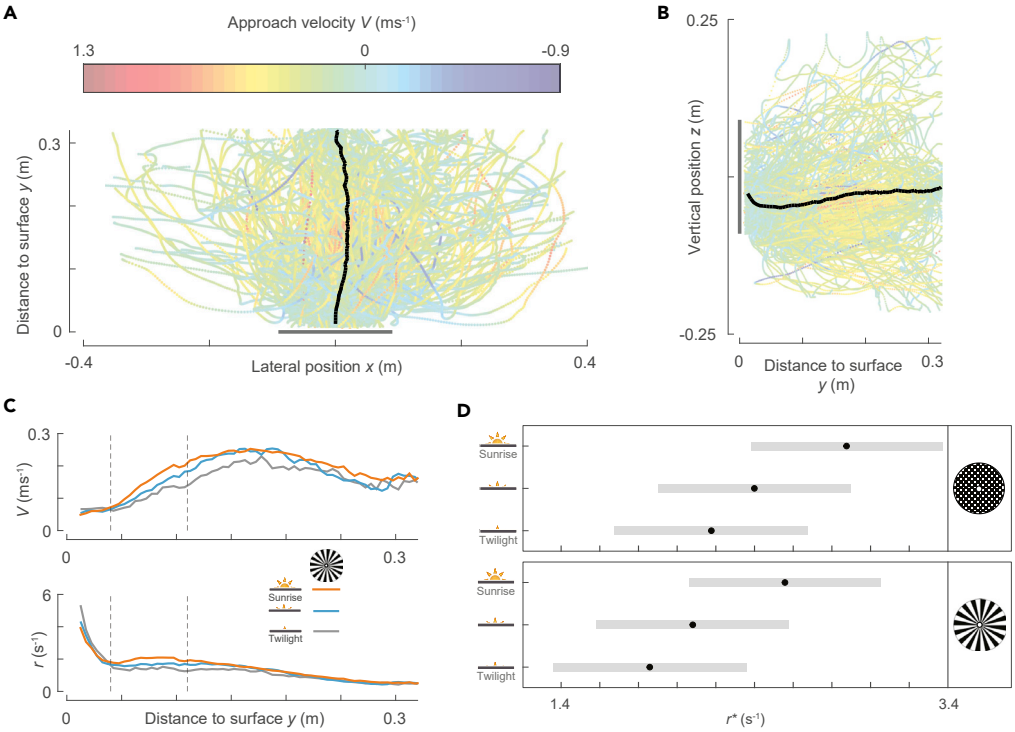

Figure 3. The average flight kinematics of bumblebees approaching a landing platform.

(A and B) Top and side views of every 35th flight trajectory of all 10,005 recorded landing maneuvers (n = 288 tracks), color-coded with approach velocity V. The black curve shows the mean trajectory of all 10,005 recorded maneuvers, and the landing platform is shown in gray.

(C and D) The average approach kinematics of bumblebees. (C) The approach velocity V and relative rate of expansion r versus perpendicular distance from the platform y for bumblebees approaching a spoke pattern for landings initiated from free flight in low, medium, and high light conditions (in gray, blue, and orange, respectively). The y segment (0.04 m $\leq y \leq$ 0.11 m) for which the data are used to find the mean relative rate of expansion r^* is highlighted in dashed black lines. (D) r^* as predicted by the linear mixed-effects model for the three tested light conditions and two landing patterns for landings of free-flying bumblebees (see methods). The mean relative rate of expansion increases with increase in light intensity but did not differ significantly between the two tested landing platforms (Table S2). Black dots depict estimated means, and gray bars are 95% confidence intervals. (See also Figures S2 and S3 and Table S2).

We used a linear mixed-effects model to test how this set point of the relative rate of expansion r^* differed between tested treatments (light condition and landing platform) and between landings following takeoff and free flight (landing type) (see methods). This showed that the set point of the relative rate of expansion r^* differed significantly between both light conditions and landing type, but r^* did not differ between the landing patterns (Table S2). The relative rate of expansion set point was higher in brighter light conditions (Figures 3C, 3D, and S3), and it was higher in landings after takeoff than in landings from free flight (Figure S3). It implies that, in the presence of brighter light conditions and when the landing followed takeoff, bumblebees decelerated more quickly during the landing maneuver, thus allowing for higher approach velocities and more rapid landings.

The expansion rate set points of the landing maneuvers across all tested conditions were on average r^* = 2.32 [0.24] s^{-1} and r^* = 3.02 [0.24] s^{-1} for the free flight landings and the landings following takeoff, respectively (mean [standard error], n = 6 conditions). These values are similar to the expansion rate set points observed in landings of honeybees (Baird et al., 2013) and the set points suggested for *Bombus impatiens* landings (Chang et al., 2016).

The flight kinematics of individual landing maneuvers

Although the average approach dynamics suggests that bumblebees use a constant relative rate of expansion landing strategy as described previously (Chang et al., 2016), we observed that individual flight trajectories deviated often significantly from the average constant relative rate of expansion track (Figure 3C). In

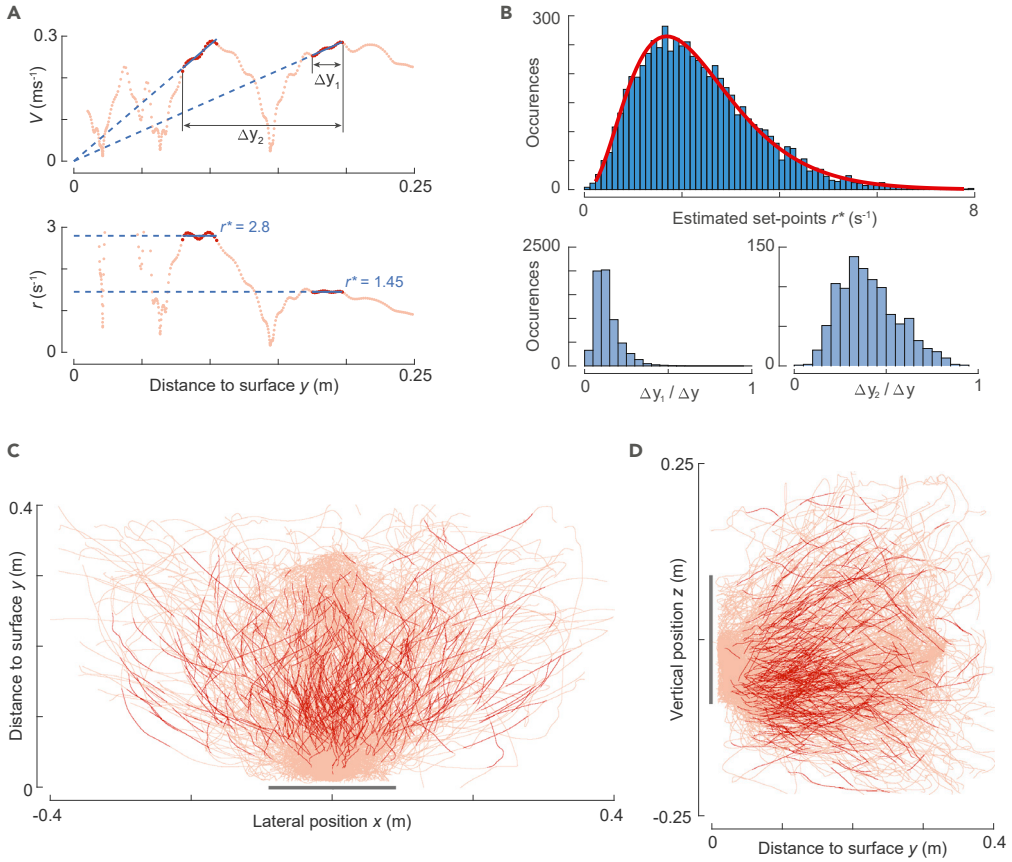

Figure 4. Landing bumblebees decelerate at a range of set points of relative rate of optical expansion (*r).**

(A) The variation of approach velocity *V* and relative rate of expansion *r* with perpendicular distance from the platform *y* of the landing maneuver in Figures 2D–2F. The segments in which *r* is identified as (nearly) constant are highlighted in dark red. The corresponding relative rate of expansion set points *r** are indicated by the dashed blue lines (as slope and ordinate values in the *V*-*y* and *r*-*y* graphs, respectively).

(B) Top panel: histogram of the set points of relative rate of expansion *r** for all identified constant-*r* segments (n = 6291 segments). Bottom panels: histograms of the ratio of displacement traveled by bumblebees during constant-*r* segments (Δy_1 or Δy_2) to the total displacement normal to the landing platform (Δy). Left shows the relative distance traveled during a single constant-*r* segment $\Delta y_1/\Delta y$ (n = 6291 segments), and right shows the relative distance traveled during two consecutive constant-*r* segments $\Delta y_2/\Delta y$ (n = 1015 segments), as defined in the panel (A).

(C and D) Top and side views of 470 tracks (every 10th of 4672 tracks) used to study the landing dynamics. The complete flight tracks are shown in orange, and the track segments in which the optical expansion rate is kept constant are highlighted in red. The landing platform is shown in gray. (See also Figures S1 and S4 and Table S3).

fact, many landing maneuvers consisted of multiple deceleration phases (Figures 2D–2F) instead of a single continuous one. To analyze these individual flight maneuvers separately, we used an in-house developed automatic detection algorithm to extract the segments of the landing maneuvers in which bumblebees kept the relative rate of expansion constant (Figure 4A, see methods for details).

Hereafter, we refer to the track segments identified using our detection algorithm as *constant-r segments* and characterize them by their average values of the four state variables (y^*,V^*,A^*,r^*), displacement normal to the platform (along *y* axis) during a single constant-*r* segment (Δy_1) and displacement normal to the platform for a set of consecutive constant-*r* segments (Δy_2) (Δy_1 and Δy_2 are annotated in Figure 4A). We use r^* as an estimate of the set point of the relative rate of expansion that the bumblebee aims to hold constant (see methods for explanation).

The output of the constant-*r* detection algorithm depends on a setting parameter *f*, whereby higher *f* leads to the detection of more (and wider) constant-*r* segments and thus fewer false negatives and more false

positives (see methods for details). We therefore performed a sensitivity analysis by systematically varying the factor f from 0.25 to 2.5 to determine its effect on the distribution of set points identified and their dynamics with distance described later in this section (see methods).

For $f = 1$, we identified 6,291 constant-r segments within the 4,672 landing maneuvers (1359 and 3313 landings starting from takeoff and free flight, respectively) out of a total of 10,005 maneuvers (Figures 4B–4D and S1). For $f = 2.5$, the number of constant-r segments increased to 16,322 constant-r segments identified within 7951 landing maneuvers. Although the number of constant-r segments increased with f, the distribution of constant-r segments (including their dynamics with distance) remained essentially unaltered throughout our tested range of f, so here, we report all results for factor $f = 1$ (see methods and Table S1 for results at the other f values).

Landing maneuvers consist of multiple flight segments with constant-r

The set points of the relative rate of expansion varied considerably among segments (Figures 4B and S4), and their observed distribution can be approximated by the gamma distribution (median $r^* = 2.15\ s^{-1}$, $a = 3.59$ [3.47–3.71], $b = 0.65$ [0.63–0.67], mean [95% confidence intervals], see methods for details).

For the 6,291 identified constant-r segments, the displacement during a single segment (Figure 4B) was $\Delta y_1 = 0.035 \pm 0.017$ m (mean $\pm$ standard deviation), which consisted on average of only 13% of the total displacement (along y-direction) during the complete approach maneuver ($\Delta y = 0.266 \pm 0.063$ m, Figure 4B). This suggests that bumblebees, while approaching a landing platform, do not fly at a single set point of the relative rate of expansion, like observed in the average-per-treatment analysis. Instead, they fly at a constant relative rate of expansion for relatively short travel distances (0.035 m), after which they likely switch to a new set point of the relative rate of expansion.

Landing bumblebees increase the constant-r set points when approaching the landing platform

We tested how bumblebees adjusted these set points of the relative rate of expansion within a landing approach by analyzing the transitions from one set point to the next, for all landing maneuvers in which we detected multiple constant-r segments (Figure 5). Out of 4,672 landing maneuvers, 1015 maneuvers were identified with two constant-r segments (examples in Figures 5A and 5B) and 283 maneuvers with three or more constant-r segments (example in Figure 5C).

The displacement during two consecutive constant-r segments (Figure 4B) was on average $\Delta y_2 = 0.114 \pm 0.049$ m ($n = 1015$ landings) and thus explained on average 40% of the total approach displacement (Figure 3D). Because the mean approach displacement during a single constant-r segment (Δy_1) was 13%, bumblebees traversed approximately 1/3rd of the displacement during two consecutive constant-r segments (Δy_2) while transitioning from one set point to another. Of all transitions between two consecutive constant-r segments, 72% of them were from a lower constant-r set point value to a higher value, and the average set point increase was $\Delta r^* = 1.05 \pm 0.93\ s^{-1}$ ($n = 1050$ transitions). Thus, during a transition, bumblebees tend to increase the set point of the relative rate of expansion (on average 113%), and a set of two consecutive constant-r segments represents a significant proportion (40%) of the total displacement during a landing maneuver. These results are consistently observed for each tested treatment and for both landing types (after takeoff and from free flight) (Table S3).

The stepwise increase of the relative rate of expansion set points occurs at a constant time-to-contact rate

The dynamics of increasing set points of the relative rate of expansion with decreasing distance from the landing platform (Figure 5) resembles the trend observed in birds that use the constant $\dot{\tau}$ landing strategy (Figure 1C). We tested whether bumblebees comply to this strategy by fitting a linear mixed-effects model (see methods) to both the data set with the maneuvers containing multiple constant-r segments (Figure 5D, Table S4, n = 2917 segments) and the complete data set (Figures 6A–6C, Table S5, n = 6,291 segments). The model predicts an average time-to-contact rate $\dot{\tau} = -0.78$ and $\dot{\tau} = -0.87$ for the reduced data set and complete data set, respectively. Thus, bumblebees increase the set points of the relative rate of expansion while approaching the landing platform at a constant time-to-contact rate. The resulting average time-to-contact rate at which they do this is strikingly similar to that observed in birds ($\dot{\tau} = -0.76$ for hummingbirds [Lee et al., 1991] and $\dot{\tau} = -0.72$ for pigeons [Lee et al., 1993]).

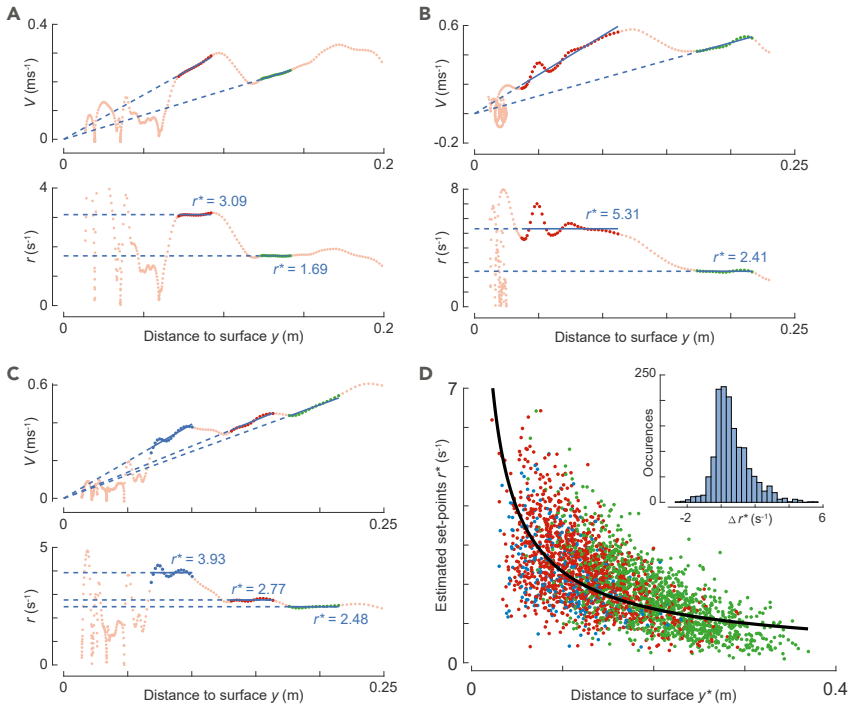

Figure 5. Bumblebees stepwise increase their set points of relative expansion rate during a landing approach.
(A–C) Examples of landing approaches that start from a free-flight condition and contain multiple set points of relative rate of expansion, as shown by the variation of approach velocity *V* and relative rate of expansion *r* with perpendicular distance from the platform *y*. The track segments in which *r* is approximately constant are highlighted in green (first observed set point), red (second set point), and blue (third or higher set point). The magnitudes of the relative rate of expansion set points *r** are indicated by the dashed blue lines (as slope and ordinate values in the *V*-*y* and *r*-*y* graphs, respectively).
(D) Variation of relative rate of expansion set point *r** with distance from the platform *y** for landing maneuvers with multiple constant-*r* segments. The first set point in each track is shown in green, the second set point in red, and third or higher set points in blue. The average variation of *r** with *y** as estimated from the linear mixed-effects model is shown in black (see methods). The inset shows a histogram of the change in relative rate of expansion set point between two consecutive constant-*r* segments Δr^* (n = 1456). (See also Tables S3 and S4).

Our linear mixed-effects model analysis also allowed us to test how the landing strategy differed with light intensity, optical expansion information of the landing platform, and between landings performed from free flight and landings that followed takeoff (Figure 6, Table S5). The minimal linear mixed-effects model included effects of all treatments and landing type but no interactions between these (see methods for details). Therefore, we here discuss the effects of light intensity, landing pattern, and landing type consecutively.

In high light intensities, bumblebees approach the landing platform at higher speeds

Our linear mixed-effects model analysis shows that the relative rate of expansion set point differed significantly between all light conditions, but the set point *r** did not differ significantly with the interaction between light intensity and *y** (Table S5). As a result, the model predicts that for an average landing maneuver, the relative rate of expansion set point at the average distance *y** = 0.15 m equals *r** = 1.68 [0.05] s^{-1}, *r** = 1.82 [0.05] s^{-1}, and *r** = 1.99 [0.05] s^{-1} in low, medium, and high light condition, respectively (mean [standard error]). This corresponds to an average approach flight speed of *V** = 0.25 [0.01] m s^{-1}, *V** = 0.27 [0.01] m s^{-1}, and *V** = 0.30 [0.01] m s^{-1} in low, medium, and high light condition, respectively. In contrast, the variation of *r** with *y** did not change with light condition, showing that the governing time-to-contact rate for adjusting set points with distance did not change with light intensity. Thus, bumblebees approached the landing platform on average 19% faster in the bright sunrise light conditions than in twilight, but the bumblebees slowed down at a similar rate in various light conditions.

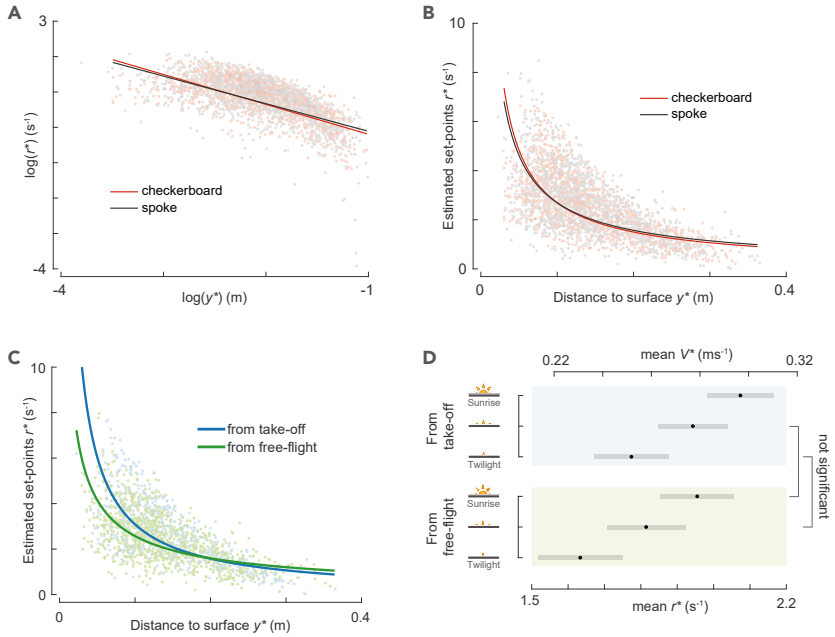

Figure 6. In all tested conditions, landing bumblebees stepwise increase their set points of relative expansion rate such that they approximate a constant time-to-contact rate landing strategy.

(A and B) The set points of relative rate of expansion r^* versus perpendicular distance from the landing platform y^*, for all detected constant-r segments in landings of freely-flying bumblebees in sunrise light, when landing on a checkerboard platform (red) or a spoke platform (gray). Data are shown in the log-transformed domain (A) and the untransformed domain (B).

(C) Variation of r^* with y^* for all detected constant-r segments of landings on a spoke landing platform in sunrise light, when initiated from takeoff (blue) and from free flight (green). (A-C) Data points show all detected constant-r segments in the condition defined by color, and the solid lines show the linear mixed-effects model fits in the log-transformed domain for the same condition.

(D) The relative rate of expansion r^* and approach flight speed V^* at the average distance from the landing platform (y^* = 0.15 m), as predicted by the model for landings directly after takeoff (top) and from free flight (bottom), and at low, medium, and high light conditions. The approach speed at y^* = 0.15 m increases with increasing light intensity and is higher for landings initiated after takeoff (Table S5 for p values). Black dots depict estimated means and gray bars are 95% confidence intervals. Non-significant differences are indicated on the right. Equivalent data for the other combinations of environmental conditions and landing types are available in Table S5.

Bumblebees brake more rapidly when landing on a platform with low optical expansion information

The statistical results related to the effect of landing platform pattern on the landing dynamics is opposite to that of light intensity: the relative rate of expansion set point at the mean distance y^* = 0.15 m did not differ significantly between landings on the different platforms but did differ significantly with the interaction between landing pattern and distance from the platform y^* (p = 0.00025, Table S5). Based on this, the statistical model predicts that, for an average bumblebee, the time-to-contact rate is 11% smaller when approaching a checkerboard landing platform with high optical expansion information ($\dot{\tau}$ = −0.92 [0.02]) than when approaching a spoke landing platform with low optical expansion information ($\dot{\tau}$ = −0.83 [0.02]).

This shows that bumblebees approaching a spoke landing platform with low optical expansion cues slowed down more quickly (higher $\dot{\tau}$) than bumblebees landing on a checkerboard platform with high optical expansion information. This results in lower approach speeds close to the landing platform, suggesting that bumblebees land more carefully on the less conspicuous platform.

Bumblebees landing from free flight brake more rapidly than bumblebees landing after takeoff

We finally tested how the landing strategy differed between landings that were performed directly after taking off and landings from free flight. The linear mixed-effects model shows that the relative rate of

expansion set point differed significantly with both landing type and the interaction between landing type and y^* ($p < 0.0001$, Table S5). The model predicts that an average bumblebee slowed down more quickly (higher $\dot{\tau}$) when landing from free flight ($\dot{\tau} = -0.73$ [0.01]) than when landing after takeoff ($\dot{\tau} = -1.01$ [0.02]) (Figure 6C). This shows that bumblebees that land from free flight start their approach flight at a higher approach velocity, but because they decelerate more quickly, they end their approach at a lower approach velocity (Figure 6C). As a result of this rapid deceleration, the approach velocity close to the platform ($y^* = 0.05$ m) is 31% lower when landing from a free flight ($V^* = 0.197$ [0.006] m s^{-1}) than when landing after takeoff ($V^* = 0.287$ [0.010] m s^{-1}).

DISCUSSION

Here, we studied how bumblebees (*B. terrestris*) decelerate to land smoothly when performing foraging flights. This includes landings that directly follow after taking off and landings that are initiated from a free flight. These two landing types represent two common but possibly distinct landing maneuvers. The landing directly after takeoff is performed by foraging bumblebees at rates of up to a 1000 times per hour when moving between flowers in a single flower patch (Heinrich, 1979); the landing from free flight is commonly performed when moving between flower patches and the hive.

To study the landing dynamics of both types of maneuvers, we trained bumblebees to forage for food. They landed on two vertical platforms directly from free flight (7213 landings) or after taking off from the opposite platform or ground (2792 landings). We placed the landing platforms 0.34 m apart, similar to the average 0.33 m distance between consecutively visited fresh flowers by bumblebees within a patch (Heinrich, 1979).

We systematically varied the visual pattern on the landing platforms (low and high optic expansion information), and we varied the environmental light intensities from twilight to sunrise conditions. Although we use vertical landing platforms, the deceleration strategy described in our study is based on an optic flow profile generated for landings on surfaces of any orientation and for any direction of approach (Baird et al., 2013).

Average landing approach kinematics versus approach kinematics of individual bumblebees

To examine how bumblebees decelerated during a landing approach, we use two different analysis methods, referred to as average-per-treatment and per-track analysis methods.

In the average-per-treatment method, we first analyzed the mean of all 10,005 approaches and selected a range of distance interval ($0.04 \text{ m} \leq y \leq 0.11$ m) in which the approach velocity toward the platform decreased proportionately with distance. Within this distance range, we then analyzed how the mean relative rate of expansion varied with tested treatment (landing pattern and light intensity) and between landing type (from takeoff or from free flight).

In the per-track analysis method, we first extracted the segments in which a bumblebee kept its relative rate of expansion constant (this constant is referred to as the relative rate of expansion set point) within each landing approach and then analyzed how the mean relative rate of expansion of all identified segments varies with the distance to the landing surface, for different treatments, and between landing types. It should be noted that the per-track analysis is inclusive of average-per-treatment analysis, i.e., if individual landing maneuvers are similar to the average landing approach, per-track analysis will identify constant-r segments only near the distance interval selected for the average-per-treatment analysis and will yield negligible dependence of set point on distance.

Using the average-per-treatment analysis – a method used in previous studies (Baird et al., 2013; Chang et al., 2016) – we found that bumblebees on average approached the platform by first increasing their velocity and then decelerated by decreasing their velocity linearly with distance to make a soft touchdown. This suggests that our bumblebees approach the landing platform by flying at a constant relative rate of expansion, as has also been described in honeybees (Baird et al., 2013) and suggested in other bumblebees (Chang et al., 2016).

The mean set point of relative rate of expansion differed between light conditions and landing type, but not between landing platforms (Figures 3C, 3D, and S3). At higher light intensities and for landings initiated

from takeoff, the rate of expansion set point was higher, resulting in a higher mean approach velocity. As a result, landings after takeoff were on average 30% faster than landings initiated from free flight, and landings in the highest light condition (sunrise) were on average 29% faster than in the lowest twilight condition.

The mean expansion rate set point at sunrise is similar to that of honeybees (8% lower for the checkerboard pattern and 15% lower for the spoke pattern) (Baird et al., 2013), but 34% lower than for *B. impatiens* bumblebees (unreported and estimated from Figure 2A in Chang et al., 2016). This striking difference in expansion rate set point could be due to differences in light conditions, as we here showed that light intensity affects the relative rate of expansion set point. However, we cannot test this because light intensity was not reported in the previous studies (Baird et al., 2013; Chang et al., 2016). A second explanation could be the differences in maximum distance available in front of the landing platform, which was 0.41 m in our setup, 1.5 m for the honeybees study (Baird et al., 2013), and 6 m for the *B. impatiens* study (Chang et al., 2016). Although our free-flight landings are initiated at speeds similar to those of *B. impatiens* (Chang et al., 2016), a new study in which landing distance is varied systematically would be needed to test this.

The hybrid landing strategy of short-distance landing maneuvers in bumblebees

The average-per-treatment analysis provided a useful insight into the mean approach dynamics but failed to capture the approach dynamics of all individual landing maneuvers. Specifically, it missed the deceleration phases that were spread across a landing approach. To capture all deceleration phases, we used our custom-developed per-track analysis method. Using this analysis, we extracted 6,291 segments (within the 4,672 landings) in which individual bumblebees kept their relative rate of expansion constant (constant-*r* segments); for each segment, we estimated the relative rate of expansion set point at which the animal flew. The distribution of these 6,291 set points reveals that landing bumblebees exhibit a skewed distribution of set points in all tested treatments (Figures 3C and S5). The observed distribution of set points encompasses the set points from average-per-treatment analyses and the ones observed for honeybees and bumblebees in earlier studies (Baird et al., 2013; Chang et al., 2016).

To determine the switching dynamics of constant-*r* set points within a landing approach, we analyzed the set point variation with distance for 1,298 approaches in which we detected more than one constant-*r* segment (Figure 5D). We found that, within a landing approach, bumblebees most often switched from a lower set point of relative rate of expansion to a higher one as this was the case in 72% of all observed transitions, and the average set point after transition was 113% higher than before. This shows that the observed wide range of set points of relative rate of expansion is not due to the individual differences between bumblebees but that the bumblebees can exhibit more than one constant-*r* set point within a single landing approach. Moreover, these dynamics are very similar between tested treatments and landing types (Table S3), indicating that the internal process of switching the set points within a landing approach happens with the same probability irrespective of both environmental conditions and landing type.

To determine how bumblebees collectively adjusted their relative rate of expansion set points as they approached the landing platforms, we tested the variation of set points of relative rate of expansion (r^*) with distance to the platform (y^*) for the 6,291 detected constant-*r* segments. We found a linear relationship between the log transformations of r^* and y^*, suggesting that bumblebees increase their set points during deceleration at a constant time-to-contact rate (Figures 1B, 1C, and 6A). These estimates of time-to-contact rate in bumblebees varied from −0.690 to −1.054 for all tested treatments and landing types and are thus similar to those observed in hummingbirds ($\dot{\tau} = -0.76$) (Lee et al., 1991) and pigeons ($\dot{\tau} = -0.72$) (Lee et al., 1993) (the reported time-to-contact rates from literature are transformed to sign convention depicted in Figure 2C). The key difference between deceleration strategies of bumblebees and birds is that birds regulate their relative rate of expansion continuously at a negative time-to-contact rate, whereas bumblebees adjust the set points of relative rate of expansion in steps at a negative time-to-contact rate, thereby discretely approximating the constant-$\dot{\tau}$ strategy of birds (Figure 1).

The adjustment of set points with distance is observed in data sets with landing maneuvers in which we detected only multiple constant-*r* segments (Table S4), only a single constant-*r* segment (Table S6) and when both data sets were pooled together (Table S5). This strongly indicates that tracks containing only one constant-*r* segment may also have more constant-*r* segments that were not detected due to the limitations of our constant-*r* extraction method. These limitations can occur due to the factor *f* that restricts the variation of *r* allowed in a constant-*r* segment (see methods), or the fundamental basis of the per-track analysis

methodology that detects only the set points that bumblebees have been able to reach and follow in their trajectory. We overcome both of these limitations by using a large data set with thousands of landing approaches.

Here, we conclude that bumblebees effectively use a hybrid between the constant-*r* landing strategy described in honeybees (Baird et al., 2013) and the constant-$\dot{\tau}$ landing strategy observed in birds (Lee et al., 1991; Lee et al., 1993), as they exhibit several segments of constant-*r* and regulate the set points of these constant-*r* segments in a constant-$\dot{\tau}$ manner.

The hybrid landing strategy is faster than a constant-*r* landing strategy

It has been suggested that the constant-$\dot{\tau}$ deceleration strategy used by birds results in faster approach flights than the constant-*r* strategy used by honeybees (Baird et al., 2013). We tested how the here-described hybrid landing strategy compares to both strategies. For this, we calculated for the 1008 landings with two consecutive constant-*r* segments, the hybrid-to-constant-*r* speed ratio and the hybrid-to-constant-$\dot{\tau}$ speed ratio as U_H/U_r and $U_H/U_{\dot{\tau}}$. Here, U_H is the average flight speed during the combined flight segment, and U_r and $U_{\dot{\tau}}$ are the equivalent speeds if the bumblebee would have used the constant-*r* and constant-$\dot{\tau}$ strategy, respectively (see methods for details). The constant-*r* and constant-$\dot{\tau}$ are based on the first set point in a set of two consecutive constant-*r* segments and average time-to-contact rate observed in our data set, respectively. For 1008 landings with two detected constant-*r* segments, the hybrid-to-constant-*r* speed ratio is $U_H/U_r = 1.16 \pm 0.69$ and the hybrid-to-constant-$\dot{\tau}$ speed ratio is $U_H/U_{\dot{\tau}} = 0.88 \pm 0.55$. This shows that the here-described hybrid landing strategy of bumblebees is 16% faster than if the bumblebee would use the equivalent constant-*r* strategy, but 12% slower than if it would continuously fly at a constant-$\dot{\tau}$. The reduction in effective flight speed relative to the true constant-$\dot{\tau}$ observed in birds is because bumblebees keep relative rate of expansion constant for some time and experience transition dynamics between two consecutive set points.

Robustness of the hybrid landing strategy of bumblebees

To test the robustness of the hybrid strategy, we offered the bumblebees different light conditions ranging from twilight to sunrise, and allowed them to land on two different landing platforms, one with a checkerboard pattern and one with a spoke pattern. We find that bumblebees robustly exhibit this strategy in all tested conditions, but with significant differences.

During constant-*r* segments, our statistical model predicts that at the average distance from the landing platforms ($y^* = 0.15$ m), bumblebees fly slower at lower light conditions, with differences ranging from 8% to 18% among different tested light conditions and for two landing types (Figures 6D, Table S5). However, the slope ($\dot{\tau}$ estimates) of regulating the set points (r^*) with distance (y^*) is not significantly different between light conditions. This shows that bumblebees tend to fly at lower speeds under lower light intensity but that the governing set point dynamics does not change with light condition. This finding is similar to the results from our average-per-treatment analysis (Figure 3D) and suggests that as light intensity falls, bumblebees possibly use neural temporal summation to improve the reliability of visual cues, and they thus fly slower to compensate for the resulting loss of temporal resolution (Baird et al., 2015; Reber et al., 2015). It is congruent with the observation in cruising flights of bumblebees (*B. terrestris)* (Reber et al., 2015) where they also reduce their mean flying speed with a decrease in light intensity.

In contrast to the negligible effect of light on set-point dynamics, the visual expansion information of the landing platform does affect the effective time-to-contact rate at which the landing bumblebees change their set points. When approaching the spoke landing platform with low visual expansion information, the bumblebees fly at 10% higher time-to-contact rate than when approaching the checkerboard platform with high expansion information. As a result, bumblebees approaching a landing platform with limited optic expansion cues decelerate more rapidly, which results in a lower approach velocity when they reach the landing platform, thus reducing the chance of collision with the surface. Because theoretically r^* can be set in the brain of a bumblebee, independent of r (a sensory measurement), bumblebees slow down more quickly and, thus, perform a more careful landing when less visual expansion information is present. These results are similar to the behavior described in honeybees where they approached a spoke landing platform at a 4% lower average relative rate of expansion than a checkerboard pattern (Baird et al., 2013).

Differences in the landing strategy between landings from free flight and after takeoff

In our study, we recorded two types of landing maneuvers, the landing directly after a takeoff and the landing initiated from free flight. We tested how these two landing types that are both commonly performed by foraging bumblebees differ.

We find that, for both types of landing maneuvers, bumblebees use the here-described hybrid landing strategy, but especially the time-to-contact rates that govern set point adjustment with distance are strikingly different (Figure 6C). Bumblebees that land from free flight exhibited on average a 28% higher time-to-contact rate than when they landed directly after takeoff. Moreover, bumblebees that land from free flight start their landing maneuver at a higher approach velocity, but because they decelerate more quickly (with 28% higher time-to-contact rate), their approach velocity at landing is much lower than for the landings after takeoff (31% lower speed at $y^* = 0.05$ m). This shows that landings from free flight are performed much more carefully than landings following takeoff, similarly to landings on a platform with low and high visual expansion cues, respectively.

The fact that these rapid consecutive takeoff and landing maneuvers are performed much more commonly by the foraging bumblebees could explain these differences as bumblebees might have learned to perform such frequent landings both rapidly and safely. A similar type of learning has been described in foraging honeybees, where honeybees that forage in an unfamiliar environment improve their in-flight aerodynamic braking in time to increase their landing success (Muijres et al., 2020).

Differences in the landing strategy between honeybees and bumblebees

Considered together, our results describe a deceleration strategy of *Bombus terrestris* during landing that is different from the deceleration strategy suggested previously for *Bombus impatiens* (Chang et al., 2016) and observed in *Apis mellifera* (Baird et al., 2013). These differences could exist due to differences among species, tested light conditions, maximum distance available in front of the landing platform, or analysis methods. It is unlikely that the differences in distance available in front of the platform is the primary cause because the bumblebees in our setup flew at approach velocities similar to the cruising speeds reported in previous bumblebee studies (Reber et al., 2015; Chang et al., 2016) (Figures 5A–5C). Light condition could possibly explain differences in the magnitude of the relative rate of expansion set point, but it is unlikely that it explains the difference between the hybrid and constant-r landing strategy among studies. Thus, the differences among species and analysis method are the most likely candidates for explaining the occurrence of two distinct landing strategies. Because our per-track analysis is more comprehensive than the average-per-treatment analysis used in literature, it would be interesting to apply our analysis method to the landing dynamics of *Apis mellifera ligustica* and *Bombus impatiens* to rule out any effect of analysis methods on observed deceleration strategies.

There is one previous honeybee landing study that used an individual track-based analysis method (Srinivasan et al., 2000). This study showed that when honeybees land on a horizontal surface, they reduce their forward flight speed linearly with distance to the surface and, thus, do not make use of the here-described hybrid landing strategy. This suggests that the landing strategy difference between our study and that described in literature (Srinivasan et al., 2000; Baird et al., 2013; Chang et al., 2016) is due to differences in species. But note that forward-flying honeybees land on horizontal surfaces by regulating front-to-back translatory optic flow, instead of optic expansion cues (Baird et al., 2013). Therefore, to conclusively determine the cause of the differences in landing strategies used by our bumblebees and honeybees, one would need to apply our analysis method to the landings that honeybees control using optical expansion cues.

How do bumblebees execute the hybrid landing strategy?

There is another important remaining question: during the hybrid landing approach, what triggers switching from one constant-r set point to another? This question is especially relevant because optical flow cues, such as visual expansion, capture the ratio of velocity and distance but do not allow disentangling these quantities. The dynamics of the transitions may provide a clue here. Most transitions look relatively smooth, but especially when closer to the landing surface, oscillations in r around the set point are evident (Figure 5). Moreover, among the 1015 tracks containing two constant-r segments, as many as 23% of the transitions contained near-zero approach velocity ($V < 0.05$ m s^{-1}). These observations point to the direction of a recent theory on monocular distance perception (de Croon, 2016), which postulates that insects can detect

the instabilities that arise when performing closed-loop optical flow control. It was shown that (de Croon, 2016), given a fixed control system, these instabilities arise at specific distances from the target object, allowing disentangling distance and speed. In the current case, the detection of instabilities could provide the bumblebee an estimate of distance to the surface which consequently could trigger the change in set point. However, alternative explanations are possible, such as the use of other distance cues (de Croon et al., 2021) or parallax cues arising from lateral motion (Baird et al., 2021). More research is needed to shed further light on this essential part of the hybrid landing strategy.

How can bumblebees estimate the relative rate of expansion?

The studies depicting neural measurements of relative rate of expansion (or time to contact) are scarce and we are aware of only one example of computation of threshold time-to-contact value by the neural system in pigeons (Wang and Frost, 1992; Sun and Frost, 1998). However, when an animal approaches a surface, it can use some measure of absolute-rate of expansion (or simply, rate of expansion ρ) (e.g., ρ averaged over a part of visual field, maximum ρ in the visual field) as a proxy for relative rate of expansion (Baird et al., 2013). Also, neural measurements of absolute rate of expansion have been recorded in honeybees (Ibbotson et al., 2017). It is therefore likely that certain neurons in bumblebees' visual neuropil also measure absolute rate of expansion which could then be used as an alternate for relative rate of expansion.

Conclusion

By using our custom-designed individual-track-based analysis method, we here described the deceleration strategy that bumblebees exhibit during landing. Specifically, we have shown that landing bumblebees decrease their velocity toward the landing platforms by holding the relative rate of optic expansion cue constant for only short bouts within the landing maneuver. From one bout to the next, they tend to increase the optic-expansion set point at which they fly. This modular increase in set points with reducing distance results in a discrete approximation of the deceleration strategy of birds. Birds use a constant time-to-contact rate to regulate their expansion rate with distance, which results in relatively fast landings.

The landing strategy of bumblebees is observed in the presence of variable degrees of optic expansion cues and is exhibited by bumblebees landing both after takeoff and from free flight. Moreover, it occurs in a wide range of luminance levels, suggesting that bumblebees adequately control landing by using neural summation. Our results are a step toward detailed understanding of how bumblebees robustly control their landing approaches. Once sufficiently understood, these control strategies can provide bioinspiration for the development of landing algorithms in autonomously flying robots.

Limitations of the study

Limitations of our relative rate of expansion set point analysis method

Our analyses assume that the sensorimotor control system of landing bumblebees sets the set points of relative rate of expansion as a goal in the brain of the bumblebee. This assumption needs to be further investigated and supported by neuroethological studies that are aimed at identifying the neural circuits that underlie this sensorimotor control system. The response property of set point identified in this study, i.e., its modulation with distance, can be useful for this purpose.

Based on the above assumption, we analyzed the landing dynamics of foraging bumblebees using two analysis methods, namely the *average-per-treatment* method and the *per-track* analysis method. Both methods provide useful insights but also have their specific limitations as described below.

Limitations of our analysis method based on the average landing dynamics

The average-per-treatment analysis method allows us to estimate the average set points of relative rate of expansion in each treatment group. This provided a useful insight into the mean approach dynamics of bumblebees and allows testing of how this differs between conditions (treatments). In contrast, the methods ignore the detailed landing dynamics exhibited by individual bumblebees. Specifically, it does not capture the rapid deceleration phases that occur in between phases at which the animal would aim to fly at a constant relative rate of expansion. To analyze these detailed flight dynamics, we developed our analysis method based on the individual flight trajectories.

Limitations of our analysis method based on the individual flight trajectories

The per-track analysis method allowed us to identify the hybrid landing strategy described in this study, but the method has one primary limitation. Because the per-track analysis method identifies set points of relative rate of expansion in individual flight trajectories, a set point can only be identified if the bumblebee flies at this set point for a certain time period. Bumblebees can fail to reach a set point for several reasons. For example, the animal can land before reaching it, the animal could switch to a new set point before reaching the previous set point, or a landing can be aborted prior to it. In our study, we identified 6,291 set points of relative rate of expansion (for $f = 1$) within 10,005 landing maneuvers, suggesting that bumblebees regularly do not fly at their expansion-rate set point.

The ability to detect a set point of relative rate of expansion depends on the sensitivity of our per-track analysis method, set by the *f*-factor (see methods). The number of identified set points increases with *f* factor, but also the number of false-positive set points increases. Based on our sensitivity analysis, we showed that the main conclusions of our study are relatively insensitive to the *f*-factor value (see methods).

In conclusion, our per-track analysis method does not allow us to identify all set points of relative rate of expansion during a landing maneuver. But because our analysis is based on a large number of flights, this does not limit us in identifying and accurately describing the hybrid landing strategy of bumblebees.

Resource availability

Lead contact

Florian T. Muijres, De Elst 1, 6708 WD, Wageningen, the Netherlands (+31 317 486 977, florian.muijres@wur.nl)

Materials availability

All materials related to this paper have been included in the paper.

Data and code availability

The data gathered during experiments are available in Mendeley Data: https://dx.doi.org/10.17632/rrbjyhkm8z.1 and the code used in the analysis is available in https://github.com/kaku289/nimble-bbee-analysis/tree/rref.

METHODS

All methods can be found in the accompanying transparent methods supplemental file.

SUPPLEMENTAL INFORMATION

Supplemental information can be found online at https://doi.org/10.1016/j.isci.2021.102407.

ACKNOWLEDGMENTS

This project is supported by the Nederlandse Organisatie voor Wetenschappelijk Onderzoek - Toegepaste en Technische Wetenschappen (NWO-TTW grant number 15039). We thank Emma Rietveld and Lana de Vries for useful discussions and help during the experiments, Henk Schipper for his help in organizing the computational resources, and Andres Hagmayer for his help with the statistical analysis. We thank Remco Huvermann, Edwin Muijt, and Anne Mathijssen from Koppert B.V. for providing the bumblebee colony. We also thank them together with Coby van Dooremalen for their advice on working with bumblebees.

AUTHOR CONTRIBUTIONS

Conceptualization, P.G., G.C.H.E.d.C., and F.T.M.; methodology, P.G. and F.T.M.; Software, P.G.; validation, P.G., M.J.L., and F.T.M.; formal analysis, P.G., J.L.v.L., and F.T.M.; investigation, P.G., A.C., and R.P.M.P.; resources, J.L.v.L., F.T.M.; data curation, P.G.; writing – original draft, P.G. and F.T.M.; writing – review & editing, P.G., A.C., G.C.H.E.d.C., M.J.L., J.L.v.L., R.P.M.P., and F.T.M.; visualization, P.G.; supervision, J.L.v.L. and F.T.M.; project administration, P.G. and F.T.M.; funding acquisition, G.C.H.E.d.C. and F.T.M..

DECLARATION OF INTERESTS

The authors declare no competing interests.

Received: October 16, 2020
Revised: February 21, 2021
Accepted: April 6, 2021
Published: May 21, 2021

REFERENCES

Baird, E., Boeddeker, N., Ibbotson, M.R., and Srinivasan, M.V. (2013). A universal strategy for visually guided landing. Proc. Natl. Acad. Sci. U S A *110*, 18686–18691. https://doi.org/10.1073/pnas.1314311110/.

Baird, E., Fernandez, D.C., Wcislo, W.T., and Warrant, E.J. (2015). Flight control and landing precision in the nocturnal bee Megalopta is robust to large changes in light intensity. Front. Physiol. *6*, 1–7. https://doi.org/10.3389/fphys.2015.00305.

Baird, E., Boeddeker, N., and Srinivasan, M.V. (2021). The effect of optic flow cues on honeybee flight control in wind. Proc. R. Soc. B Biol. Sci. *288*, 20203051. https://doi.org/10.1098/rspb.2020.3051.

Balebail, S., Raja, S.K., and Sane, S.P. (2019). Landing maneuvers of houseflies on vertical and inverted surfaces. PLoS One *14*, 1–17. https://doi.org/10.1371/journal.pone.0219861.

Van Breugel, F., and Dickinson, M.H. (2012). The visual control of landing and obstacle avoidance in the fruit fly *Drosophila melanogaster*. J. Exp. Biol. *215*, 1783–1798. https://doi.org/10.1242/jeb.066498.

Chang, J.J., Crall, J.D., and Combes, S.A. (2016). Wind alters landing dynamics in bumblebees. J. Exp. Biol. *219*, 2819–2822. https://doi.org/10.1242/jeb.137976.

Corbet, S.A., Fussell, M., Ake, R., Fraser, A., Gunson, C., Savage, A., and Smith, K. (1993). Temperature and the pollinating activity of social bees. Ecol. Entomol. *18*, 17–30. https://doi.org/10.1111/j.1365-2311.1993.tb01075.x.

de Croon, G.C.H.E. (2016). Monocular distance estimation with optical flow maneuvers and efference copies: a stability-based strategy. Bioinsp. Biomim. *11*, 016004. https://doi.org/10.1088/1748-3190/11/1/016004.

de Croon, G.C.H.E., De Wagter, C., and Seidl, T. (2021). Enhancing optical-flow-based control by learning visual appearance cues for flying robots. Nat. Mach. Intell. *3*, 33–41. https://doi.org/10.1038/s42256-020-00279-7.

Edwards, M., and Ibbotson, M.R. (2007). Relative sensitivities to large-field optic-flow patterns varying in direction and speed. Perception *36*, 113–124. https://doi.org/10.1068/p5626.

Fontaine, C., Dajoz, I., Meriguet, J., and Loreau, M. (2006). Functional diversity of plant-pollinator interaction webs enhances the persistence of plant communities. PLoS Biol. *4*, 0129–0135. https://doi.org/10.1371/journal.pbio.0040001.

Foster, D.J., and Cartar, R.V. (2011). What causes wing wear in foraging bumble bees? J. Exp. Biol. *214*, 1896–1901. https://doi.org/10.1242/jeb.051730.

Gibson, J.J. (1955). The optical expansion-pattern in aerial locomotion. Am. J. Psychol. *68*, 480–484. https://doi.org/10.2307/1418538.

Heinrich, B. (1979). Resource heterogeneity and patterns of movement in foraging bumblebees. Oecologia *40*, 235–245. https://doi.org/10.1007/BF00345321.

Ibbotson, M.R., Hung, Y.S., Meffin, H., Boeddeker, N., and Srinivasan, M.V. (2017). Neural basis of forward flight control and landing in honeybees. Sci. Rep. *7*, 1–15. https://doi.org/10.1038/s41598-017-14954-0.

Joar Hegland, S., and Totland, Ø. (2008). Is the magnitude of pollen limitation in a plant community affected by pollinator visitation and plant species specialisation levels? Oikos. .080227085440234–0. https://doi.org/10.1111/j.2008.0030-1299.16561.x.

Lee, D.N. (1976). A theory of visual control of braking based on information about time to collision. Perception *5*, 437–459. https://doi.org/10.1068/p050437.

Lee, D.N., Davies, M., and Green, P. (1993). Visual control of velocity of approach by pigeons when landing. J. Exp. Biol. *180*, 85–104.

Lee, D.N., Bootsma, R., Frost, B., Land, M., Regan, D., and Gray, R. (2009). Lee's 1976 paper. Perception *38*, 837–858. https://doi.org/10.1068/pmklee.

Lee, D.N., Reddish, P.E., and Rand, D.T. (1991). Aerial docking by hummingbirds. Naturwissenschaften *78*, 526–527. https://doi.org/10.1007/BF01131406.

Reber, T., Vähäkainu, A., Baird, E., Weckström, M., Warrant, E., and Dacke, M. (2015). Effect of light intensity on flight control and temporal properties of photoreceptors in bumblebees. J. Exp. Biol. *218* (9), 1339–1346. https://doi.org/10.1242/jeb.113886.

Muijres, F.T., van Dooremalen, C., Lankheet, M., Lugt, H., de Vries, L.J., and Van Langevelde, F. (2020). *Varroa destructor* infestation impairs the improvement of landing performance in foraging honeybees. R. Soc. Open Sci. *7*, 201222. https://doi.org/10.1098/rsos.201222.

Reber, T., Dacke, M., Warrant, E., and Baird, E. (2016). Bumblebees perform well-controlled landings in dim light. Front. Behav. Neurosci. *10*, 1–10. https://doi.org/10.3389/fnbeh.2016.00174.

Srinivasan, M.V., Zhang, S.W., Chahl, J.S., Barth, E., and Venkatesh, S. (2000). How honeybees make grazing landings on flat surfaces. Biol. Cybern. *83*, 171–183. https://doi.org/10.1007/s004220000162.

Straw, A.D., Branson, K., Neumann, T.R., and Dickinson, M.H. (2011). Multi-camera real-time three-dimensional tracking of multiple flying animals. J. R. Soc. Interf. *8*, 395–409. https://doi.org/10.1098/rsif.2010.0230.

Sun, H., and Frost, B.J. (1998). Computation of different optical variables of looming objects in pigeon nucleus rotundus neurons. Nat. Neurosci. *1*, 296–303. https://doi.org/10.1038/1110.

Velthuis, H.W., and van Doorn, A. (2006). A century of advances in bumblebee domestication and the economic and environmental aspects of its commercialization for pollination. Apidologie *37*, 421–451, https://doi.org/10.1051/apido:2006019.

Wagner, H. (1982). Flow-field variables trigger landing in flies. Nature *297*, 147–148. https://doi.org/10.1038/297147a0.

Wang, Y., and Frost, B.J. (1992). Time to collision is signalled by neurons in the nucleus rotundus of pigeons. Nature *356*, 236–238. https://doi.org/10.1038/356236a0.

iScience, Volume *24*

Supplemental information

Bumblebees land rapidly and robustly using a sophisticated modular flight control strategy

Pulkit Goyal, Antoine Cribellier, Guido C.H.E. de Croon, Martin J. Lankheet, Johan L. van Leeuwen, Remco P.M. Pieters, and Florian T. Muijres

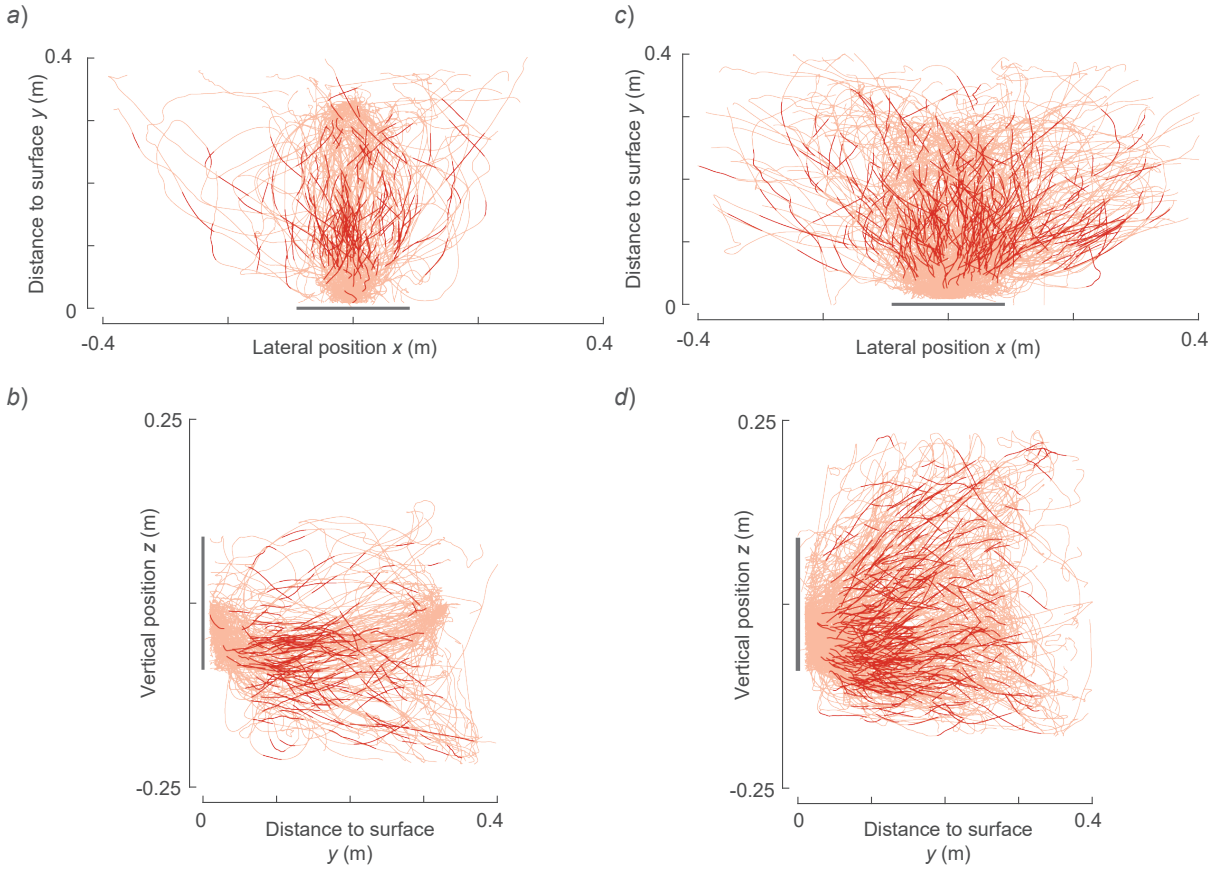

Figure S1: Flight trajectories of bumblebees landing directly after take-off (a,b) and from free-flight (c,d) (related to Figure 4). (a,b) Top and side views of 138 flight trajectories of bumblebees that landed immediately after taking-off from either the ground or the opposite platform (every 10^{th} of 1359 flight tracks are shown). (c,d) Top and side views of 334 flight trajectories of bumblebees that initiated landing from a free-flight (every 10^{th} track of 3313 recorded tracks are shown). (a-d) The flight tracks, landing platform, and the track segments in which optical expansion rate is kept constant are shown in orange, grey, and red, respectively.

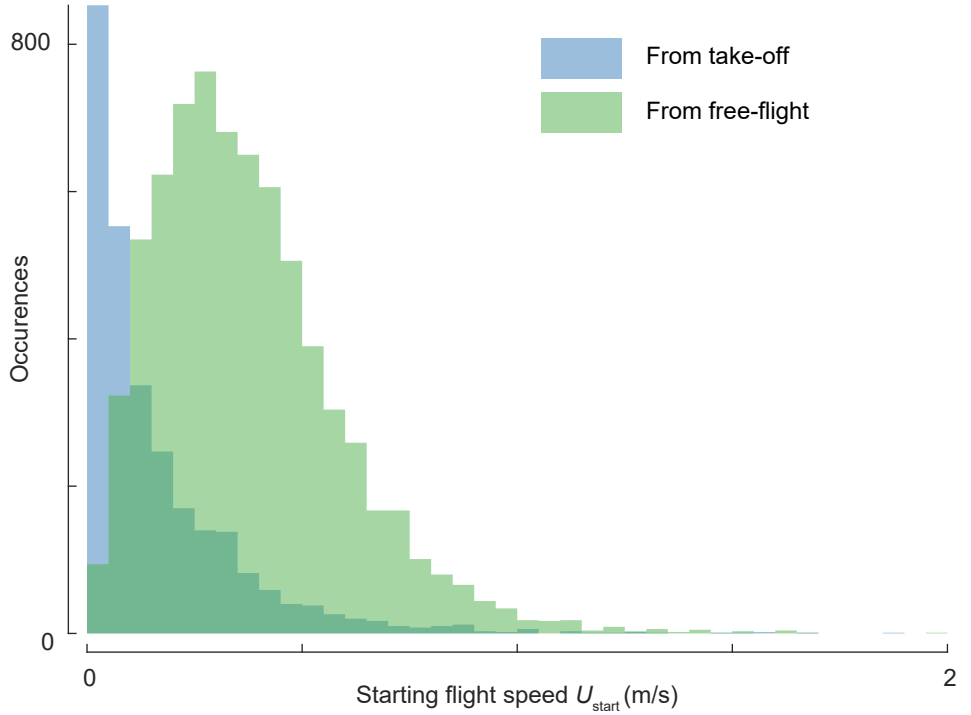

Figure S2: Histogram of flight speeds at the start of the landing manoeuvres performed by bumblebees from take-off (blue, n=2792) and from free-flight (green, n=7213) (related to Figure 3).

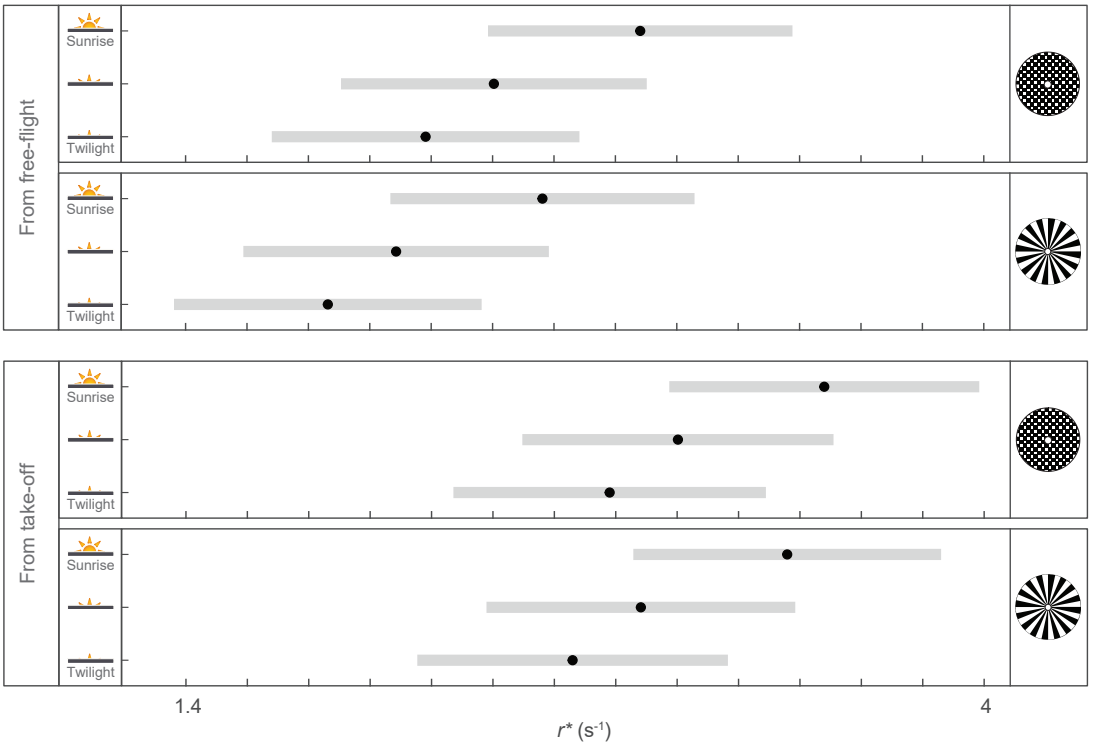

Figure S3: The mean relative-rate-of-expansion *r as predicted by the linear mixed-effects model in three tested light conditions and two landing patterns for both landing types (from take-off and free-flight) using average-per-treatment analysis (related to Figure 3)**. The mean relative-rate-of-expansion increases with increase in light intensity and is higher when bumblebees initiate landing from take-off. It did not differ significantly between the two tested landing platforms (Table S2). Black dots depict estimated means and grey bars are 95% confidence intervals.

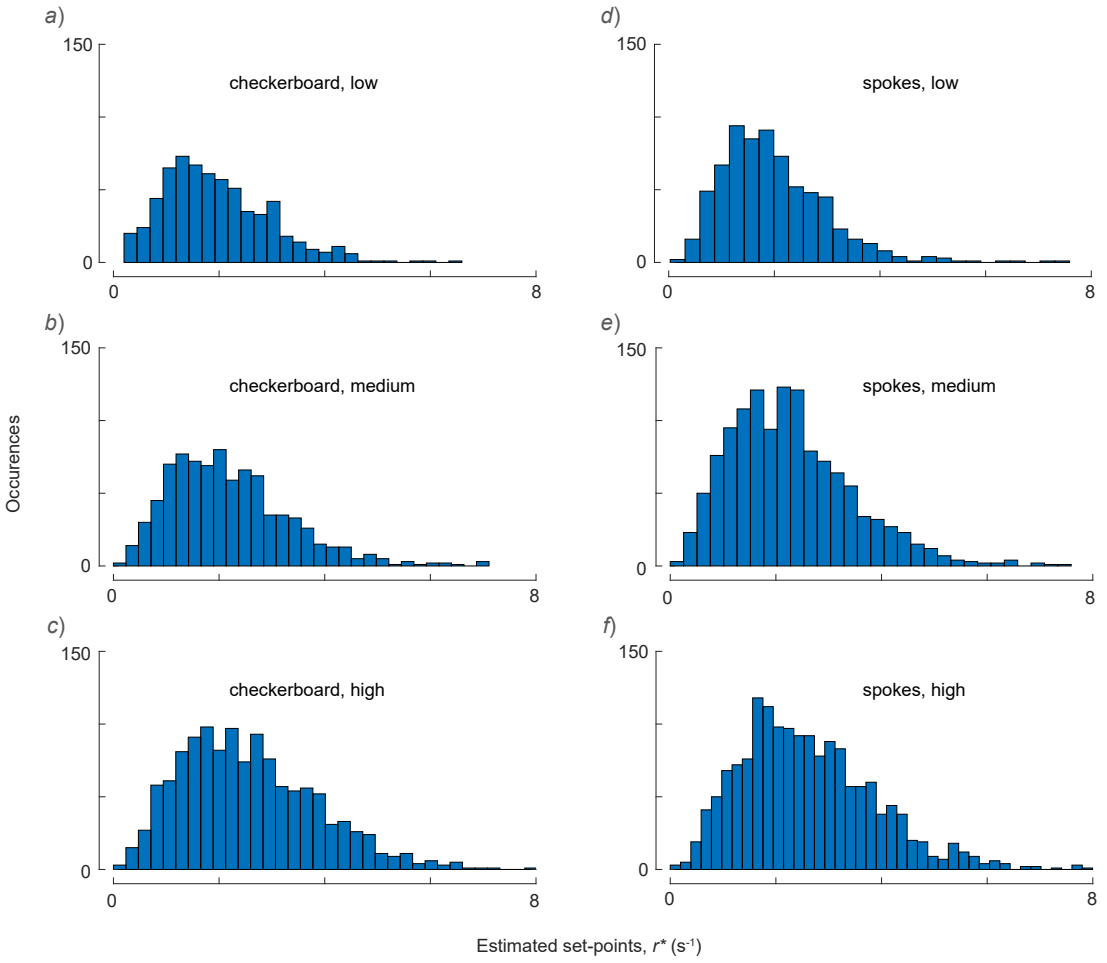

Figure S4: Histograms of the set-points of optical expansion rate r^* in all tested treatments (related to Figure 4). The conditions are: (a) checkerboard pattern, low light condition (n=643 segments), (b) checkerboard pattern, medium light condition (n=847 segments), (c) checkerboard pattern, high light condition (n=1243 segments), (d) spoke pattern, low light condition (n=700 segments), (e) spoke pattern, medium light condition (n=1255 segments), (f) spoke pattern, high light condition (n=1603 segments). (a-f) Each panel contains set-points for both landing types (landings initiated from take-off and free-flight).

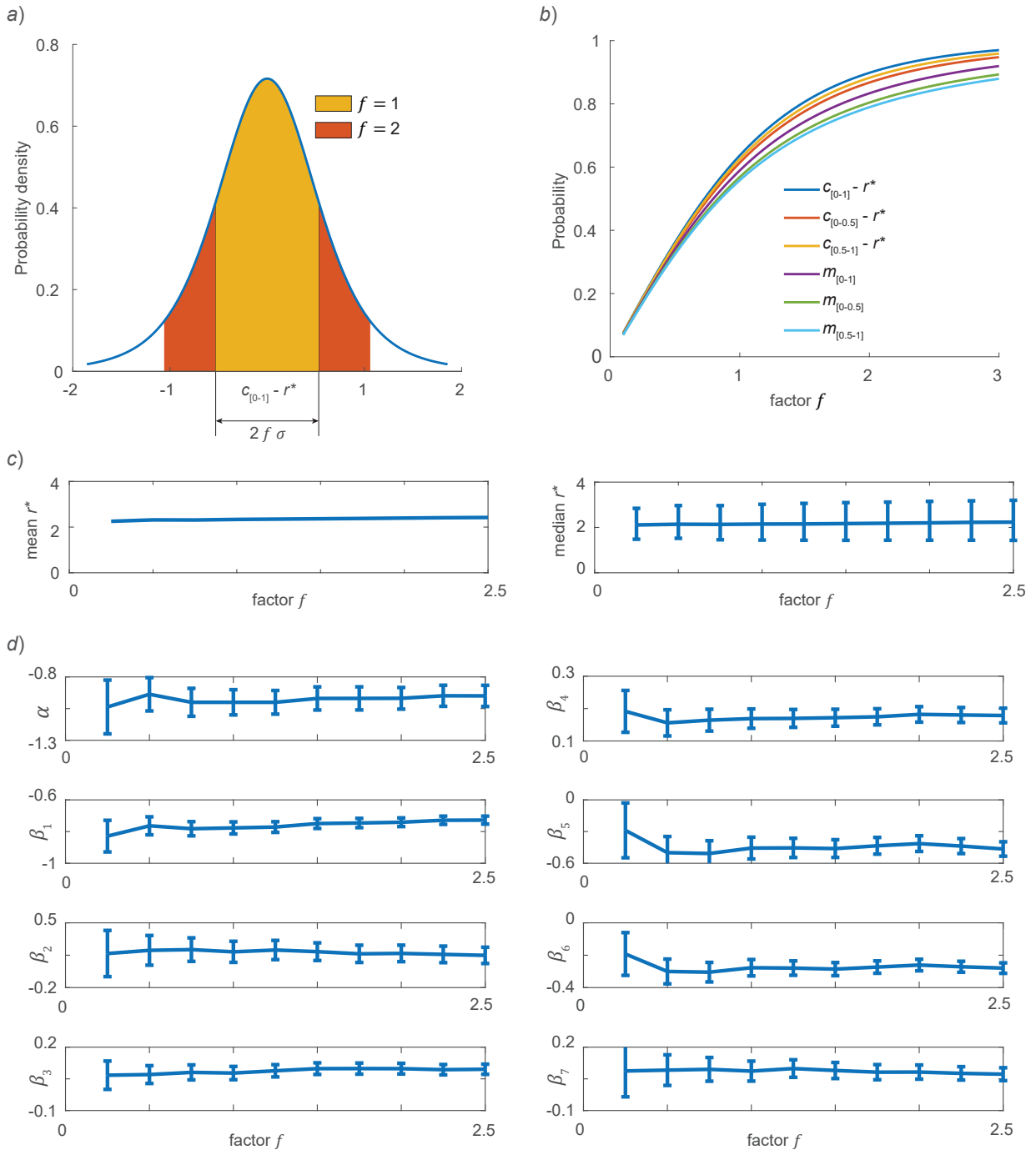

Figure S5: The effect of factor f on the results (related to Figures 4 – 6). (a) The threshold of variation allowed around the mean for $f = 1$ (yellow) and $f = 2$ (orange) for the probability density function of parameter $c_{[0-1]} - r^*$, $\sigma = 0.53$. (b) The probability of values that lie within f scale-parameter band around the mean of each parameter ($c_{[0-1]} - r^*$, $c_{[0-0.5]} - r^*$, $c_{[0.5-1]} - r^*$, $m_{[0-1]}$, $m_{[0-0.5]}$, and $m_{[0.5-1]}$). (c) The mean and median, 25 percentile and 75 percentile of the set-points of relative-rate-of-expansion identified at various values of the factor f. (d) The dependence of r^* on distance from the platform (y^*) along with the effect of different environmental conditions (landing patterns and light conditions) and landing type (take-off or free-flight) as per Equation S2 for each factor ($\log(r^*_{i,d,a,s}) \sim N(\alpha + \alpha_d + \alpha_a + \alpha_s + \beta_1 \ \log(y^*_{i,d,a,s}) + \beta_2 \ \text{SPOKE}_{i,d,a,s} + \beta_3 \ \text{MEDIUMlight}_{i,d,a,s} + \beta_4 \ \text{HIGHlight}_{i,d,a,s} + \beta_5 \ \text{fromTakeoff}_{i,d,a,s} + \beta_6 \ \log(y_{i,d,a,s}) \times \text{fromTakeoff}_{i,d,a,s} + \beta_7 \ \log(y_{i,d,a,s}) \times \text{SPOKE}_{i,d,a,s}, \ \sigma^2)$, vertical bars for each coefficient indicate 95% confidence intervals).

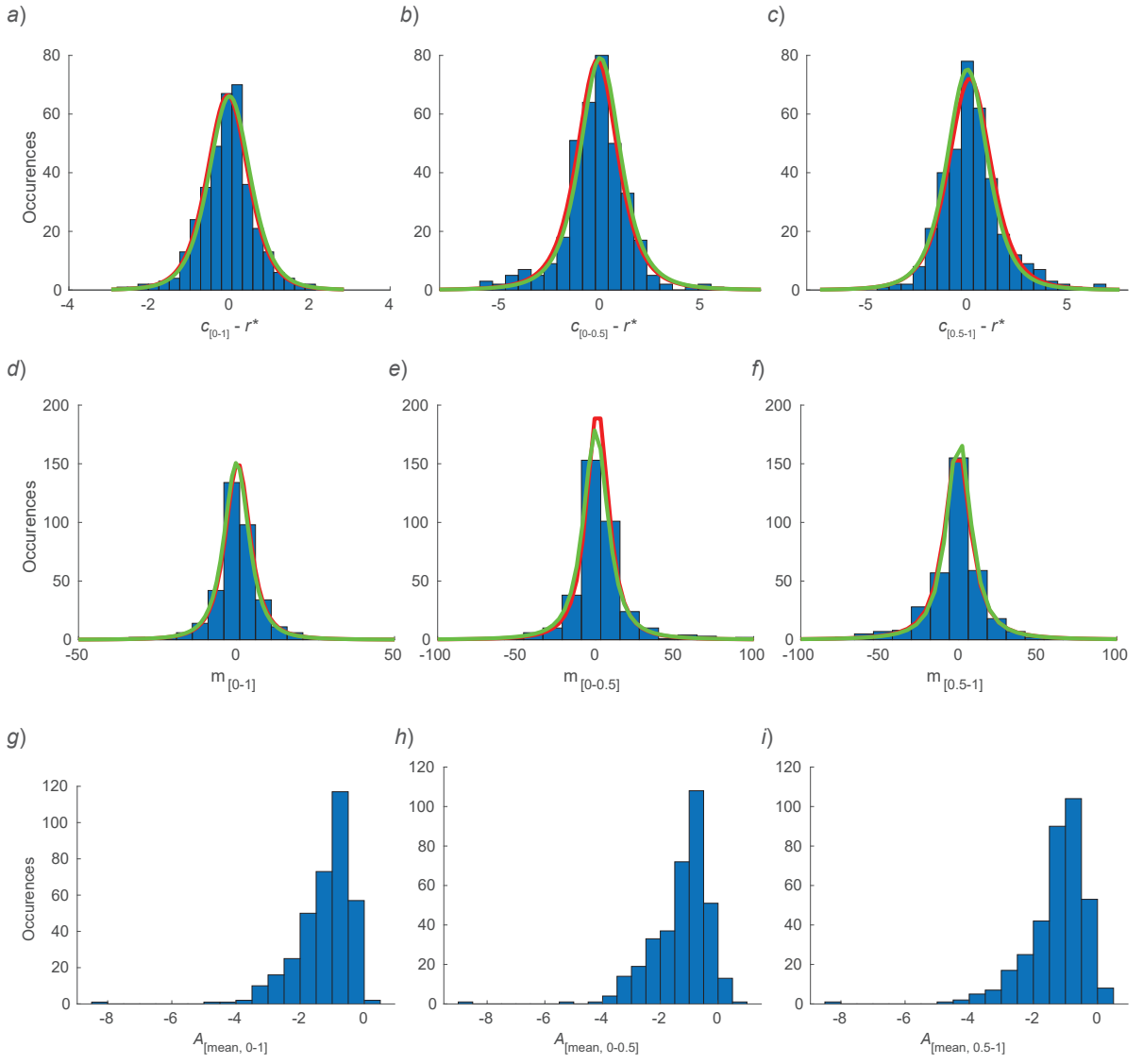

Figure S6: Distributions of nine parameters used in the constant-r extraction algorithm (related to Figures 4 – 6). (a) $c_{[0-1]} - r^*$, (b) $c_{[0-0.5]} - r^*$, (c) $c_{[0.5-1]} - r^*$, (d) $m_{[0-1]}$, (e) $m_{[0-0.5]}$, (f) $m_{[0.5-1]}$, (g) $A_{[\text{mean},0-1]}$), (h) $A_{[\text{mean},0-0.5]}$, and (i) $A_{[\text{mean},0.5-1]}$. In blue, histograms of nine parameters obtained from manual selection of 355 constant-r segments in 313 (out of first 532) landing manoeuvres for high light condition and spoke landing pattern. In red, estimated probability density functions of first six parameters (generalized student's t-distributions, see Table S8 for parameter values). In green, the representative probability density functions of first six parameters used in constant-r extraction algorithm (location parameter μ for these six parameters is zero, scale parameter σ is σ_1, $2\sigma_1$, $2\sigma_1$, σ_2, $2\sigma_2$ and $2\sigma_2$ for panels (a)-(f), respectively (where $\sigma_1 = 0.53$ and $\sigma_2 = 4.22$) and shape parameter ν is same as in Table S8).

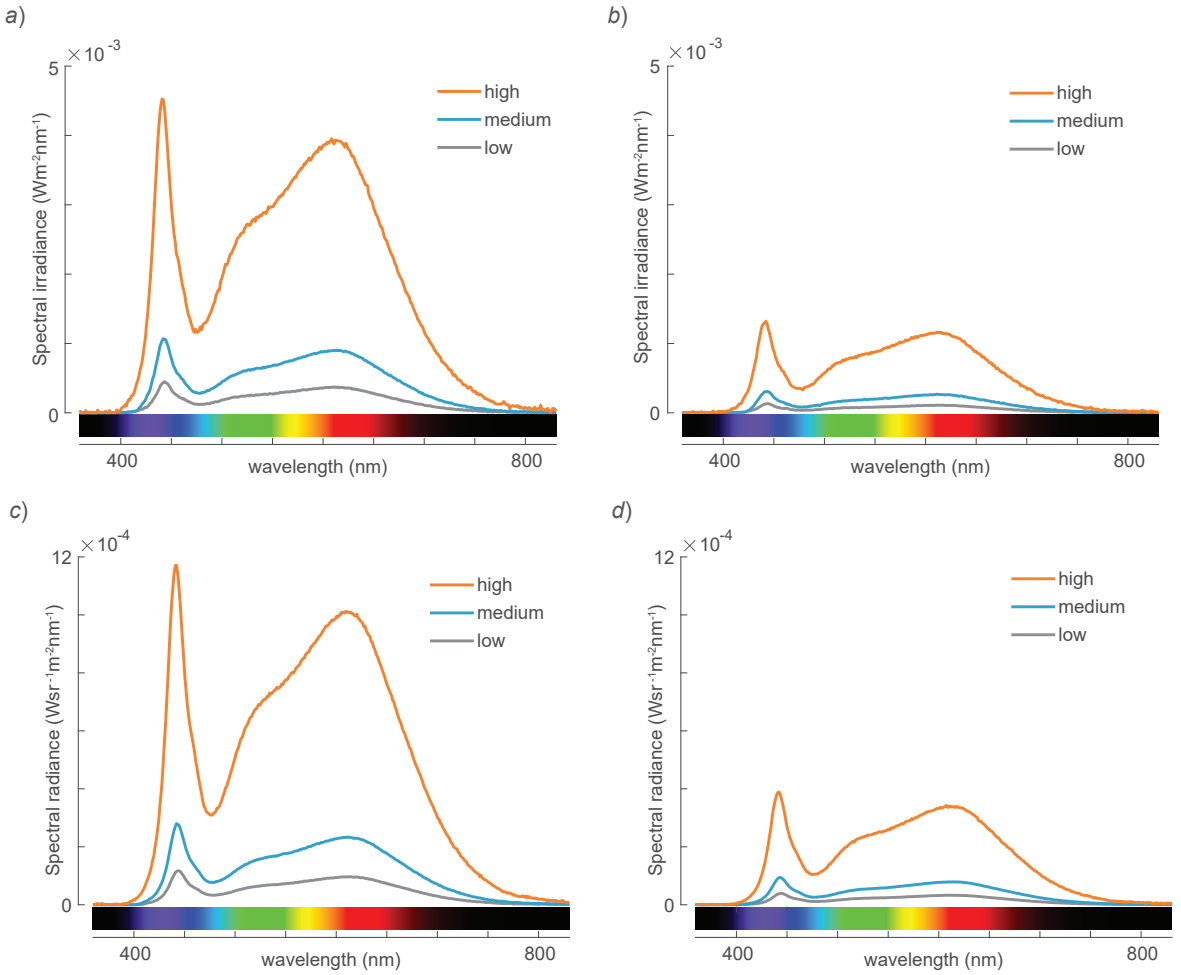

Figure S7: Light intensities for the low (grey), medium (blue) and high (orange) light conditions (related to Figure 2). Spectral irradiance (a) and spectral radiance (c) at the center of the flight arena. Spectral irradiance (b) and spectral radiance (d) at the centre of the landing platforms.

Table S1: The number of landing manoeuvres recorded in each tested treatment and the number of landing manoeuvres that are identified with constant-r segments for different values of factor f (related to Figure 4).

Treatment (landing pattern, light condition)	Number of landing manoeuvres	Factors f 0.25	0.5	0.75	1	1.25	1.5	1.75	2	2.25	2.5
From free-flight											
checkerboard, low	579	55	149	225	300	362	395	423	452	473	484
checkerboard, medium	923	71	221	358	472	545	605	649	687	719	744
checkerboard, high	1886	94	327	541	729	871	988	1099	1188	1271	1347
spoke, low	520	70	162	241	303	348	380	405	431	449	461
spoke, medium	1188	104	294	474	626	747	834	893	939	995	1027
spoke, high	2117	129	383	639	883	1065	1198	1325	1426	1521	1589
From take-off											
checkerboard, low	242	26	79	125	152	163	182	191	200	208	216
checkerboard, medium	287	24	67	96	137	169	189	203	219	230	238
checkerboard, high	554	35	99	164	229	271	312	343	377	406	422
spoke, low	298	30	88	123	166	196	224	234	250	266	271
spoke, medium	593	52	149	237	296	359	402	435	454	476	492
spoke, high	818	62	179	283	379	449	512	549	596	629	660
Total landings	10005	752	2197	3506	4672	5545	6221	6749	7219	7643	7951

Table S2: Analysis of mean relative-rate-of-expansion in different tested treatments (landing patterns, light conditions and starting conditions) for average-per-treatment analysis method (related to Figure 3). The data comprises of 10,005 landing approaches between 0.04 m $\leq y \leq$ 0.11 m, where y is the perpendicular distance to the platforms. Post-hoc tests compare differences between mean relative-rate-of-expansion observed in different tested conditions (statistical model as given by Equation S1: $\mathrm{r}_{i,d,a,s} \sim N(\alpha + \alpha_d + \alpha_a + \alpha_s + \beta_1\ \mathrm{SPOKE}_{i,d,a,s} + \beta_2\ \mathrm{MEDIUMlight}_{i,d,a,s} + \beta_3\ \mathrm{HIGHlight}_{i,d,a,s} + \beta_4\ \mathrm{fromTakeoff}_{i,d,a,s} + \beta_5\ \mathrm{SPOKE}_{i,d,a,s} \times \mathrm{fromTakeoff}_{i,d,a,s},\ \sigma^2)$).

Fixed effect	Estimate	Std error	t value	Pr(>|t|)
α	2.18	0.26	8.51	0.034
β_1	-0.32	0.15	-2.17	0.056
β_2	0.22	0.05	4.07	4.67E-5
β_3	0.70	0.05	13.90	< 2E-16
β_4	0.60	0.06	9.64	< 2E-16
β_5	0.20	0.08	2.44	0.015
Post-hoc contrasts*	Estimate	Std error	z ratio	p value
(H + F) - (L + F)	0.70	0.05	13.90	4.1E-42
(H + F) - (M + F)	0.48	0.04	11.76	3.95E-30
(H + F) - (H × F)	0.32	0.15	2.17	1
(H + F) - (L × F)	1.02	0.16	6.53	4.3E-09
(H + F) - (M × F)	0.80	0.15	5.21	1.24E-05
(L + F) - (M + F)	-0.22	0.05	-4.07	0.003054
(L + F) - (H × F)	-0.38	0.16	-2.45	0.930313
(L + F) - (L × F)	0.32	0.15	2.17	1
(L + F) - (M × F)	0.10	0.16	0.61	1
(M + F) - (H × F)	-0.16	0.15	-1.04	1
(M + F) - (L × F)	0.54	0.16	3.44	0.038107
(M + F) - (M × F)	0.32	0.15	2.17	1
(H × F) - (L × F)	0.70	0.05	13.90	4.1E-42
(H × F) - (M × F)	0.48	0.04	11.76	3.95E-30
(L × F) - (M × F)	-0.22	0.05	-4.07	0.003054
(H + T) - (L + T)	0.70	0.05	13.90	4.1E-42
(H + T) - (M + T)	0.48	0.04	11.76	3.95E-30
(H + T) - (H × T)	0.12	0.16	0.76	1
(H + T) - (L × T)	0.82	0.17	4.91	6.12E-05
(H + T) - (M × T)	0.60	0.16	3.65	0.017404
(L + T) - (M + T)	-0.22	0.05	-4.07	0.003054
(L + T) - (H × T)	-0.58	0.17	-3.48	0.033282
(L + T) - (L × T)	0.12	0.16	0.76	1
(L + T) - (M × T)	-0.10	0.17	-0.61	1
(M + T) - (H × T)	-0.36	0.16	-2.17	1
(M + T) - (L × T)	0.34	0.17	2.03	1
(M + T) - (M × T)	0.12	0.16	0.76	1
(H × T) - (L × T)	0.70	0.05	13.90	4.1E-42
(H × T) - (M × T)	0.48	0.04	11.76	3.95E-30
(L × T) - (M × T)	-0.22	0.05	-4.07	0.003054

*Low (L), medium (M) and high (H) light conditions, checkerboard (+) and spoke (×) landing patterns, free-flight (F) and take-off (T) starting conditions.

*Comparisons among starting conditions also formed part of post-hoc test, but are not shown here.

Table S3: Number of landing manoeuvres that contain more than one set-points of relative-rate-of-expansion along with different characteristics (Δr^*, Δy_1 and Δy_2, related to Figure 4 and 5) in different tested treatments (factor $f = 1$).

Treatment (pattern, light)	No. of landing tracks with constant-r segments	No. of constant-r segments	No. of manoeuvres with >1 constant-r segments	For 1298 manoeuvres with more than one constant-r segments				For 1015 manoeuvres with two constant-r segments	
				No. of constant-r segments	No. of jumps to a different r^*	For jumps to a higher r^*		$\Delta y_1(m)$ (mean [std-dev.])	$\Delta y_2(m)$ (mean [std-dev.])
						% of jumps	$\Delta r^*(s^{-1})$ (mean [std-dev.])		
From free-flight									
L+	300	418	94	212	118	73.7%	0.740 [0.688]	0.030 [0.015]	0.099 [0.040]
M+	472	667	148	343	195	72.3%	1.023 [0.964]	0.033 [0.016]	0.110 [0.044]
H+	729	939	175	385	210	74.8%	1.394 [1.120]	0.037 [0.018]	0.116 [0.053]
Lx	303	454	118	269	151	67.6%	0.778 [0.595]	0.030 [0.015]	0.107 [0.046]
Mx	626	854	180	408	228	71.5%	1.047 [0.846]	0.034 [0.018]	0.111 [0.047]
Hx	883	1103	187	407	220	75.0%	1.198 [0.964]	0.036 [0.017]	0.112 [0.047]
From take-off									
L+	152	225	54	127	73	75.3%	0.986 [0.873]	0.033 [0.018]	0.132 [0.048]
M+	137	180	37	80	43	74.4%	1.052 [1.065]	0.036 [0.019]	0.121 [0.060]
H+	229	304	64	139	75	73.3%	1.305 [1.184]	0.037 [0.017]	0.114 [0.052]
Lx	166	246	61	141	80	75.0%	0.854 [0.733]	0.035 [0.019]	0.120 [0.052]
Mx	296	401	82	187	105	72.4%	0.967 [0.892]	0.036 [0.017]	0.122 [0.053]
Hx	379	500	98	219	121	65.3%	1.221 [1.020]	0.039 [0.020]	0.128 [0.054]

Low (L), medium (M) and high (H) light conditions, checkerboard (+) and spoke (x) landing patterns.

Table S4: Analysis of relative-rate-of-expansion set-points (r^*) dependence on distance to the platform (y^*) in different tested treatments (landing patterns and light conditions) and with different starting conditions (take-off and free-flight) for per-track analysis method (related to Figure 5). The data comprises of r^* and y^* for 2,917 constant-r segments in 1,298 landing manoeuvres that contain more than one constant-r segments (factor $f = 1$) (statistical model as given by Equation S2: $\log(r^*_{i,d,a,s}) \sim N(\alpha + \alpha_d + \alpha_a + \alpha_s + \beta_1\ \log(y^*_{i,d,a,s}) + \beta_2\ \mathrm{SPOKE}_{i,d,a,s} + \beta_3\ \mathrm{MEDIUMlight}_{i,d,a,s} + \beta_4\ \mathrm{HIGHlight}_{i,d,a,s} + \beta_5\ \mathrm{fromTakeoff}_{i,d,a,s} + \beta_6\ \log(y_{i,d,a,s}) \times \mathrm{fromTakeoff}_{i,d,a,s} + \beta_7\ \log(y_{i,d,a,s}) \times \mathrm{SPOKE}_{i,d,a,s},\ \sigma^2)$).

Fixed effect	Estimate	Std error	t value	Pr(>|t|)
α	-0.98	0.06	-17.64	1.11E-47
β_1	-0.74	0.03	-28.88	5.3E-161
β_2	0.18	0.07	2.62	0.009372
β_3	0.06	0.02	2.85	0.004463
β_4	0.17	0.02	8.00	2.68E-15
β_5	-0.26	0.07	-3.76	0.000173
β_6	-0.16	0.03	-4.55	5.54E-06
β_7	0.09	0.03	2.65	0.008201

Table S5: Analysis of relative-rate-of-expansion set-points (r^*) dependence on distance to the platform (y^*) in different tested treatments (landing patterns and light conditions) and with different starting conditions (take-off and free-flight) for per-track analysis method (related to Figure 6). The data comprises of r^* and y^* for 6,291 constant-r segments in 4,672 landing manoeuvres. Post-hoc tests compare differences in $log(r^*)$ observed at mean $y^* = 0.15m$ in the presence of different light conditions and landing platforms (factor $f = 1$) (statistical model as given by Equation S2: $\log(r^*_{i,d,a,s}) \sim N(\alpha+\alpha_d+\alpha_a+\alpha_s+\beta_1\ \log(y^*_{i,d,a,s})+\beta_2\ \mathrm{SPOKE}_{i,d,a,s}+\beta_3\ \mathrm{MEDIUMlight}_{i,d,a,s}+\beta_4\ \mathrm{HIGHlight}_{i,d,a,s}+\beta_5\ \mathrm{fromTakeoff}_{i,d,a,s}+\beta_6\ \log(y_{i,d,a,s}) \times \mathrm{fromTakeoff}_{i,d,a,s}+\beta_7\ \log(y_{i,d,a,s}) \times \mathrm{SPOKE}_{i,d,a,s},\ \sigma^2)$).

Fixed effect	Estimate	Std error	t value	Pr(>|t|)
α	-1.00	0.05	-20.13	1.53E-17
β_1	-0.78	0.02	-40.76	0
β_2	0.19	0.06	3.28	0.001397
β_3	0.08	0.02	4.92	8.81E-07
β_4	0.17	0.01	11.31	3.31E-29
β_5	-0.46	0.05	-8.85	1.09E-18
β_6	-0.28	0.03	-10.93	1.44E-27
β_7	0.09	0.02	3.67	0.000248
Post-hoc constrasts* in $log(r^*)$ at mean $y^* = 0.15m$	Estimate	Std error	z ratio	p value
L F - M F	-0.08	0.02	-4.92	1.27E-05
L F - H F	-0.17	0.01	-11.31	1.72E-28
L F - L T	-0.07	0.01	-5.58	3.68E-07
L F - M T	-0.15	0.02	-7.13	1.53E-11
L F - H T	-0.24	0.02	-11.94	1.14E-31
M F - H F	-0.09	0.01	-7.17	1.1E-11
M F - L T	0.01	0.02	0.35	1
M F - M T	-0.07	0.01	-5.58	3.68E-07
M F - H T	-0.16	0.02	-9.08	1.63E-18
H F - L T	0.10	0.02	5.17	3.46E-06
H F - M T	0.02	0.02	1.17	1
H F - H T	-0.07	0.01	-5.58	3.68E-07
L T - M T	-0.08	0.02	-4.92	1.27E-05
L T - H T	-0.17	0.01	-11.31	1.72E-28
M T - H T	-0.09	0.01	-7.17	1.1E-11

*Low (L), medium (M) and high (H) light conditions, free-flight (F) and take-off (T) starting conditions.

*The results are averaged over patterns because comparisons of r^* among landing patterns for each light condition and starting condition were similar.

Table S6: Analysis of relative-rate-of-expansion set-points (r^*) dependence on distance to the platform (y^*) in different tested treatments (landing patterns and light conditions) and with different starting conditions (take-off and free-flight) for per-track analysis method (related to Figures 5 and 6). The data comprises of r^* and y^* for 3,374 constant-r segments in 3,374 landing manoeuvres, with one constant-r segment in each manoeuvre (factor $f = 1$) (statistical model as given by Equation S2: $\log(r^*_{i,d,a,s}) \sim N(\alpha + \alpha_d + \alpha_a + \alpha_s + \beta_1\ \log(y^*_{i,d,a,s}) + \beta_2\ \mathrm{SPOKE}_{i,d,a,s} + \beta_3\ \mathrm{MEDIUMlight}_{i,d,a,s} + \beta_4\ \mathrm{HIGHlight}_{i,d,a,s} + \beta_5\ \mathrm{fromTakeoff}_{i,d,a,s} + \beta_6\ \log(y_{i,d,a,s}) \times \mathrm{fromTakeoff}_{i,d,a,s} + \beta_7\ \log(y_{i,d,a,s}) \times \mathrm{SPOKE}_{i,d,a,s},\ \sigma^2)$).

Fixed effect	Estimate	Std error	t value	Pr(>|t|)
α	-0.97	0.07	-14.15	2.68E-17
β_1	-0.79	0.03	-28.56	8.2E-161
β_2	0.22	0.08	2.82	0.005261
β_3	0.08	0.02	3.49	0.000484
β_4	0.14	0.02	6.96	4.2E-12
β_5	-0.67	0.07	-8.99	4.16E-19
β_6	-0.40	0.04	-11.02	8.71E-28
β_7	0.10	0.03	3.01	0.002627

Table S7: Pseudo-random treatment schedule followed during experiments (related to Figure 2).

Time (hours)		Days													
start	end	1	2	3	4	5	6	7	8	9	10	11	12	13	14
80000	93000	M+	Lx	L+	Hx	L+	Hx	H+	Mx	H+	Mx	M+	Lx	M+	Lx
93000	110000	H+	Mx	H+	Mx	M+	Lx	M+	Lx	L+	Hx	L+	Hx	H+	Mx
110000	123000	L+	Hx	M+	Lx	H+	Mx	L+	Hx	M+	Lx	H+	Mx	L+	Hx
123000	140000	M+	Lx	L+	Hx	L+	Hx	H+	Mx	H+	Mx	M+	Lx	M+	Lx
140000	153000	H+	Mx	H+	Mx	M+	Lx	M+	Lx	L+	Hx	L+	Hx	H+	Mx
153000	170000	L+	Hx	M+	Lx	H+	Mx	L+	Hx	M+	Lx	H+	Mx	L+	Hx

Low (L), medium (M) and high (H) light conditions, checkerboard (+) and spoke (x) landing patterns.

Table S8: Estimated location parameter μ, scale parameter σ and shape parameter ν for six variables that together define the constancy of relative-rate-of-expansion in a track segment (values are mean [95% confidence intervals]) (related to Figures 4 and S6).

Variables	μ	σ	ν
$c_{[0-1]} - r^*$	-0.05 [-0.11, 0.02]	0.53 [0.46, 0.60]	5.02 [2.87, 8.77]
$c_{[0-0.5]} - r^*$	-0.14 [-0.28, -0.00]	1.07 [0.93, 1.23]	3.24 [2.20, 4.76]
$c_{[0.5-1]} - r^*$	0.12 [-0.02, 0.26]	1.11 [0.96, 1.27]	3.92 [2.47, 6.23]
$m_{[0-1]}$	0.39 [-0.16, 0.95]	4.22 [3.63, 4.91]	2.30 [1.69, 3.13]
$m_{[0-0.5]}$	1.20 [0.16, 2.24]	7.67 [6.57, 8.95]	1.82 [1.41, 2.35]
$m_{[0.5-1]}$	-0.72 [-1.93, 0.49]	8.85 [7.47, 10.48]	1.64 [1.27, 2.12]

S1. Transparent methods

S1.1. Experimental Animals

We used a commercially available hive of bumblebees (*Bombus terrestris*) from Koppert B.V. (Berkel en Rodenrijs, the Netherlands) for our experiments. The colony contained 50–70 worker bumblebees (female) that engaged in different activities required to maintain the hive. Among others, they performed foraging flights to collect artificial nectar (50% sugar solution obtained from Koppert B.V.) from a feeding platform. They had ad libitum access to the food source during the day and were given dried pollen directly in the hive at the end of each day. We placed the hive in an indoor laboratory where the temperature was maintained at 21 ± 2^{o}C and the hive remained connected to our setup for the entire duration of the experiment.

S1.2. Experimental setup

The experimental setup consisted of a flight arena ($3 \times 0.48 \times 0.48$ m; length×width×height), with a bumblebee hive, food source, and a real-time machine-vision based videography system for tracking the flying bumblebees (Figure 2a,b). The top, bottom, and longitudinal side walls of the flight arena were made of transparent poly-carbonate sheets (thickness 0.01 m) and the far ends were closed with meshes. We installed the hive and a food source (containing sugar solution) outside the flight chamber and directly opposite to each other (Figure 2a). The hive and the food-source were connected to the longitudinal walls of the flight chamber near its middle section using Plexiglas tubes. These tubes extended 0.07 m inside the flight chamber and had vertical landing platforms attached at the end (Figure 2b). The landing discs were covered with either a checkerboard pattern (0.01 m black and white squares) or spoke pattern (32 spokes filled with alternating black and white colours) (Figure 2c) printed on a normal paper.

The flight chamber was illuminated with white broad-spectrum LED light panel (Lumihome 595×595 mm, 4800 lm, LED type: SMD2835, 4000K), powered with 300W power supply (maximum 40 V and 1.1 A) (RS PRO RS6005P). This light panel was placed 50 cm above the chamber's top wall and right above the middle section of the flight arena (Figure 2a,b). The light panel could be set to three different light intensities by PWM dimming: a low light condition simulating dusk (13.7 lx), a medium light condition (33.3 lx), and a high light condition equivalent to sunrise (144.9 lx). Reported light intensities were the average at the centre of the flight arena and at the landing platforms, measured using a spectroradiometer (Specbos 1211 with JETI Lival software, Figure S7).

Flight movements of the foraging bumblebees were tracked in 3D using a real-time machine-vision based videography system. The system consisted of four synchronized high-speed cameras (one Basler acA1300-200um camera with 12 mm Fujinon lens and three Basler acA2040-90um cameras with 12.5 mm Kowa lenses), which viewed the central portion of the arena from two orthogonal positions above the arena and two orthogonal positions from the side (Figure 2a). The cameras operated at 175 frames per second, image resolution was 504×504 pixels for Basler acA2040-90um cameras and 512×512 pixels for Basler acA1300-200um camera, and image depth was 8 bits. Exposure times were 260 µs, 200 µs, 400 µs and 900 µs for top-left (Basler acA2040-90um), top-right (Basler acA2040-90um), side-left (Basler acA2040-90um), and side-right (Basler acA1300-200um) cameras, respectively. All cameras were back-lit using custom-built arrays of infrared (IR) LED panels (centroid wavelength: 850 nm) to enhance the contrast of bumblebees with the background (19.25 V, 1 A).

When running, the real-time machine-vision based videography system estimated the three-dimensional position of all moving bumblebees at each recording time step. Based on these, movement trajectories for each bumblebee were constructed. To remove tracking noise from these trajectories, we filtered these using a low-pass second-order two-directional Butterworth filter (*filtfilt* in Matlab 2020a, MathWorks Inc) with a cut-off frequency of 20 Hz, and then stored in arrays with space-time vectors $\mathbf{X}_G = (x_G, y_G, z_G, t_G)$. Position was defined in the global coordinate system (not shown), and time resolution equalled that of the videography system (1/175 s). The software also had the option to automatically store video images to disc, based on tracking output. We calibrated the videography system four times throughout the experiments using Direct Linear Transformation; a correction for lens distortion was performed once (Svoboda, Martinec and Pajdla, 2005; Straw, Branson, Neumann and Dickinson, 2011).

S1.3. Experimental procedure

Before starting the experiments, we trained the bumblebees for 10 days to forage in the arena at the low light intensity condition. At the start of the training period, we directly connected the hive and food source with a bridge, allowing the bumblebees to walk to the food source; each day, we gradually increased the bridge gap until after 10 days the forager bumblebees would comfortably fly back and forth between hive and food source.

During training and experiments, we exposed bumblebees to a day-night cycle of 10-14 hours with day starting at 07:30h and ending at 17:30h. Sunrise (07:30h–08:00h) was simulated by gradually increasing the light intensity from zero to the light condition for the experiment (low, medium or high) or training (low). Similarly, sunset (17:00h–17:30h) was simulated by gradually reducing the last light condition of the day down to zero. During experiments, the rest of the day (08:00h–17:00h) was divided into 6 time-slots of 1.5 hours each. We changed the light condition in each time-slot and landing platform every day (Table S7).

Since the recorded landing manoeuvres are likely to be highly stereotypical, we used a single hive in our study. The recorded landing manoeuvres are thus pseudo-replications of foraging bumblebees that existed in the hive over a span of 14 consecutive days.

S1.4. Extraction of landing tracks

From all trajectory data of bumblebees inside the flight arena, we first selected the tracks in which bumblebees were flying, as tracks that were less than 5% of the time closer than 6 cm from the side walls or less than 0.1% of the time closer than 5 cm from the top and bottom surfaces. Among the resulting flight tracks, we then selected the tracks in which bumblebees approached one of the landing platforms. These landing approach tracks were defined as tracks that started at a normal distance (along y-axis) of at least 10 cm from the landing platform, and had a minimum normal distance to the platform of less than 2 cm. For each track that met those criteria, the landing approach manoeuvre was selected as the trajectory section between the distance furthest away from the landing platform and closest distance (up to 1cm). Furthermore, the tracks starting close to either of the platforms (within 2.5 cm long cylinder around opposite disc) or the ground (less than 2 cm distance from ground) were labelled as the landing approaches starting from a take-off and the rest of the tracks were labelled as the landing approaches from free-flight condition.

The landing approaches were stored as space-time arrays $\mathbf{X} = (x, y, z, t)$, in the landing platform coordinate system (Figure 2c). This cartesian coordinate system has its origin at the centre of the landing platform, y normal to the platform, and z upwards. Time t was set to zero at the end of the trajectory, i.e. when the bumblebee reached the closest distance to the platform. The corresponding velocity and acceleration vectors ($\mathbf{U} = (u, v, w)$ and $\mathbf{A} = (a_x, a_y, a_z)$, respectively) were computed by numerical differentiation using a second-order central differentiation scheme and stored. These approach sequences, referred to as landing manoeuvres, were analysed in this study.

S1.5. Estimation of state variables and set-points of relative-rate-of-expansion (r^*)

To analyse the landing dynamics of bumblebees, we focused on the movement normal to the landing platform, which can be described by the state variables: normal distance from the platform $y(t)$, flight velocity towards the platform $V(t) = -v(t)$, and acceleration towards the platform $A(t) = -a_y(t)$. Based on these, we calculated the instantaneous relative rate of optical expansion throughout each landing approach track, as $r(t) = V(t)/y(t)$. In total, we thus used the temporal dynamics of four state variables (y, V, A, r) to describe the dynamics of bumblebees decelerating as they approach a surface for landing. A previous study suggested that bumblebees on an average hold the relative-rate-of-expansion constant during a landing approach (Chang, Crall and Combes, 2016). Therefore, we developed a custom-made search algorithm for automatic identification of the landing approach segments in which the relative-rate-of-expansion was close to a constant as bumblebees were decelerating.

The constant-r detection algorithm is based on six parameters that together define the constancy of r in a track segment. For an arbitrary track segment, these six parameters are computed from three first-order linear regressions (one regression in full segment, and two regressions in two equal halves of the full segment) and they evaluate the deviations of these regressions from a constant r regression. To evaluate these deviations, we first find the expected probability distributions for each of these six parameters when bumblebees were flying with constant r, and then check whether the six parameters computed for an arbitrary segment lie within certain threshold around the expected mean of each parameter. This threshold is specified by a setting parameter f whose value can be changed to alter the variation allowed around the mean of each of the six linear regression parameters for an arbitrary segment to be identified as a constant-r segment. This f is thus similar to the number of standard deviations around the mean of a normally distributed variable that is included in the selection. Hence, by finding these parameters for different track segments in a landing manoeuvre, we could identify all track segments in which a bumblebee kept the variation of r below a threshold defined by a fixed value of factor f.

The identified track segments are called constant-r segments and are characterized by their average values of the four state variables (y^*, V^*, A^*, r^*). Here, r^* is a linear regression estimate from $r(t) = r^* + \epsilon$ (where ϵ denotes residuals) within a constant-r segment, and we use it as an estimate of the set-point of relative-rate-of-expansion that

the bumblebee aims to hold constant. This is because r^* for each constant-r track segment is very close to m, where m is a linear regression estimate of $V(t) = m \times y(t) + \epsilon$ (ϵ denotes residuals) in a constant-r segment (mean, median and maximum difference between the two values are 0.005, 0.002 and 0.096 s^{-1}, respectively). Moreover, the difference between the actual flight duration and the analytically computed flight duration if the bumblebees had followed exactly the estimated set-points of relative-rate-of-expansion within identified constant-r segments is extremely low (maximum difference = 0.0086 s which is only 1.5 times 1/175 s, the time resolution of the experimental apparatus). Additionally, we only consider the velocity perpendicular to the platforms as this component of the velocity was needed to be progressively built and later progressively reduced as bumblebees approached the platforms for landing. However, the deceleration strategy of adjusting these set-points with distance remains unchanged if 3D speed is considered.

S1.6. Statistical models

All statistical analyses were done in R 4.0.2 (R Foundation). We used *lmer* to develop different linear mixed-effects models for the two analysis methods. The landing patterns, light conditions, landing type (take-off and free-flight) along with their (significant) interactions are considered as fixed factors, and day of the experiment, landing side (whether the landing disc is located towards the hive or the food-source) and each landing approach are considered as random intercepts. We used model dredging to identify the minimal linear mixed-effects statistical model. For post-hoc tests, we used Bonferroni correction (using *emmeans* package in R) to adjust the statistical significance values for comparison of means and covariates in different treatments (landing patterns and light conditions) and for different landing types. p-values < 0.05 were considered statistically significant. Unless stated otherwise, data-sets averages and distributions are given as mean±standard deviation, including sample size (n); statistical model predictions are given as mean [standard error], including p-values if relevant.

Specifically, the linear mixed-effects models were developed to determine (a) the set-points of relative-rate-of-expansion (r^*) in average-per-treatment method, (b) the set-point variation with distance from the landing platforms (y^*) in per-track method, and (c) the effect of landing patterns, light conditions and landing type (landings starting from take-off or free-flight) in both analyses.

S1.6.1. The average-per-treatment model

For the average-per-treatment analysis method, we computed the mean relative-rate-of-expansion in each tested treatment by first using pattern, light, starting conditions along with all possible interactions as fixed factors and day of the experiment, landing approach number, and landing side (whether landing disc is located on the hive side or the food source side) as random factors. The model dredging revealed only $pattern \times startingCondition$ as significant, therefore we used the reduced model (Equation S1).

$$\begin{aligned} r_{i,d,a,s} \sim N(\alpha + \alpha_d + \alpha_a + \alpha_s + \beta_1\ \mathrm{SPOKE}_{i,d,a,s} + \beta_2\ \mathrm{MEDIUMlight}_{i,d,a,s} + \beta_3\ \mathrm{HIGHlight}_{i,d,a,s} + \\ \beta_4\ \mathrm{fromTakeoff}_{i,d,a,s} + \beta_5\ \mathrm{SPOKE}_{i,d,a,s} \times \mathrm{fromTakeoff}_{i,d,a,s},\ \sigma^2) \end{aligned} \tag{S1}$$

where $r_{i,d,a,s}$ is the relative-rate-of-expansion for the i-th measurement from d-th day ($d \in \{1, 2, \ldots, 14\}$), a-th landing approach ($a \in \{1, 2, \ldots, 10005\}$) and s-th landing side ($s = 1$ for hive side and $s = 2$ for food-source side), α is the regression intercept for checkerboard pattern and low light condition (overall intercept), α_d is the day-specific intercept, α_a is the landing-approach-specific intercept, α_s is the landing-side-specific intercept, $\mathrm{SPOKE}_{i,d,a,s}$, $\mathrm{MEDIUMlight}_{i,d,a,s}$, $\mathrm{HIGHlight}_{i,d,a,s}$ and $\mathrm{fromTakeoff}_{i,d,a,s}$ indicate if spoke landing pattern, medium light condition, high light condition and take-off are present for the i-th measurement from d-th day, a-th landing approach and s-th landing side (0 = no, 1 = yes), $\beta_i\ \forall i \in \{1, 2, 3, 4, 5\}$ represent differences of fixed-effects and an interaction term from overall intercept, and σ is the residual standard deviation. The statistical output, along with post-hoc tests, from data of 10,005 landing approaches in the selected range of distance to the platforms ($0.04m \leq y \leq 0.11m$) is given in Table S2.

S1.6.2. The per-track analysis model

For the per-track analysis method, the dependence of set-points of relative-rate-of-expansion (r^*) on distance to the platform (y^*) was deemed based on the interdependence of r and y for a constant-$\dot{\tau}$ landing strategy (Equation S8b) i.e., a linear relationship between their log transformations. To adjudge the dependence of r^* on y^* as per constant-$\dot{\tau}$ law, we first constructed a full model with $\log(r^*)$ as response variable, $\log(y^*)$, landing patterns, light conditions, landing types along with all interactions as fixed factors, and day of the experiment, landing approach and landing side (whether landing disc is located on the hive side or the food source side) as random intercepts. Among all interaction terms,

the model dredging revealed only $\log(y^*) \times pattern$ and $\log(y^*) \times startingCondition$ interaction terms as significant, therefore we used the following reduced model:

$$\begin{aligned}\log(r^*_{i,d,a,s}) \sim N(\alpha + \alpha_d + \alpha_a + \alpha_s + \beta_1\ \log(y^*_{i,d,a,s}) + \beta_2\ \text{SPOKE}_{i,d,a,s} + \beta_3\ \text{MEDIUMlight}_{i,d,a,s} + \\ \beta_4\ \text{HIGHlight}_{i,d,a,s} + \beta_5\ \text{fromTakeoff}_{i,d,a,s} + \beta_6\ \log(y_{i,d,a,s}) \times \text{fromTakeoff}_{i,d,a,s} + \\ \beta_7\ \log(y_{i,d,a,s}) \times \text{SPOKE}_{i,d,a,s},\ \sigma^2)\end{aligned} \tag{S2}$$

where $r^*_{i,d,a,s}$ and $y^*_{i,d,a,s}$ are set-point of relative-rate-of-expansion and mean distance, respectively, for the i-th constant-r segment from d-th day ($d \in \{1, 2, \dots, 14\}$), a-th landing approach ($a \in \{1, 2, \dots, 4672\}$) and s-th landing side ($s = 1$ for hive side and $s = 2$ for food-source side), α is the regression intercept for checkerboard pattern, low light condition and free-flight starting condition (overall intercept), α_d is the day-specific intercept, α_a is the landing-approach-specific intercept, α_s is the landing-side-specific intercept, $\text{SPOKE}_{i,d,a,s}$, $\text{MEDIUMlight}_{i,d,a,s}$, $\text{HIGHlight}_{i,d,a,s}$ and $\text{fromTakeoff}_{i,d,a,s}$ indicate if spoke landing pattern, medium light condition, high light condition and take-off starting condition are present for the i-th measurement from d-th day, a-th landing approach and s-th landing side (0 = no, 1 = yes), β_1 represents the regression slope for predictor $\log(y^*)$ (overall slope), $\beta_i\ \forall i \in \{2, 3, 4, 5, 6, 7\}$ represent differences of fixed-effects including an interaction from overall intercept and slope, and σ is the residual standard deviation. The statistical output, along with post-hoc tests, from data of 4,672 landing manoeuvres is given in Table S5.

S1.7. Algorithm for automatic extraction of set-points of relative-rate-of-expansion

In order to automatically extract the segments of landing tracks in which bumblebees kept the relative-rate-of-expansion constant (constant-r segments), we first define methods to estimate the set-points of relative-rate-of-expansion and the variation of relative-rate-of-expansion around its estimated set-point. We later use these defined methods to construct an algorithm for automatic search of constant-r segments in each landing approach.

S1.8. Estimation of a set-point of relative-rate-of-expansion

For a track segment in which relative-rate-of-expansion is held constant, we find a zeroth-order linear regression of r to obtain the set-point (r^*) at which r is held constant (Equations S3). [align=middle]

$$r(t) = r^* + \epsilon \tag{S3a}$$

$$r^* = \frac{\sum_{i=1}^{n} r(t_i)}{n} \tag{S3b}$$

where n denotes the number of data points in that track segment and ϵ denotes the residuals. The intercept (r^*) in the linear regression is an average of the relative-rate-of-expansion observed within a constant-r segment and is used as an estimate of the set-point of r within that segment.

S1.8.1. Identification of variation around the set-points

To find the expected variation of r around the set-points in constant-r segments, we began by identifying such segments in a smaller data-set using a custom-built Graphical User Interface (GUI) in MATLAB 2020a. In this GUI, we plotted the computed state variables (V and r) against the perpendicular distance from the platform (y) and manually selected segment(s) of y (similar to the ones highlighted in red in Figure 4a) over which the instantaneous relative-rate-of-expansion (or its mean) was observed to be nearly constant. For this purpose, we use first 532 landing manoeuvres recorded for high light condition and spoke landing pattern. Out of 532 tracks, we identified 313 tracks with 355 constant-r segments (273 tracks with one segment, 38 tracks with two segments and 2 tracks with three segments) and estimated the set-point r^* using Equations S3 for each such segment.

To find the variation of r around the estimated set-points r^*, we estimated slopes and intercepts of three first-order linear fits in each such segment - one through the complete segment and two through its equal halves (Equations S4). Since, the relative-rate-of-expansion is expected to be nearly constant in the full segment and also in its two halves, the variations of three slopes, along with differences between three intercepts and the corresponding estimated set-point for the full segment, are expected to be centered around zero. We use the two halves of the segments in addition to the full segment to avoid false positives segments being detected, namely in which bumblebees are either transitioning from acceleration to deceleration phase or vice-a-versa.

$$r_{[0-1]} = m_{[0-1]}\ y_{[0-1]} + c_{[0-1]} + \epsilon \tag{S4a}$$

$$r_{[0-0.5]} = m_{[0-0.5]}\, y_{[0-0.5]} + c_{[0-0.5]} + \epsilon \tag{S4b}$$

$$r_{[0.5-1]} = m_{[0.5-1]}\, y_{[0.5-1]} + c_{[0.5-1]} + \epsilon \tag{S4c}$$

Subscripts $[0-1]$, $[0-0.5]$, and $[0.5-1]$ denote the full segment, first half, and second half of the segment, respectively, variables m and c denote the slope and intercept of a fit obtained using first-order linear regression and ϵ denotes the residuals in each case.

The distributions of three slopes ($m_{[0-1]}$, $m_{[0-0.5]}$ and $m_{[0.5-1]}$) and distributions of differences between three intercepts and the corresponding estimated set-point for the full segment ($c_{[0-1]} - r^*$, $c_{[0-0.5]} - r^*$ and $c_{[0.5-1]} - r^*$) are fitted using generalized student's t-distribution to identify their probability density functions (*tLocationScaleDistribution* in Matlab 2020a). Each such distribution is defined by a location parameter μ, scale parameter σ and shape parameter ν (σ dictates the spread of the distribution). As expected (Table S8), the location parameter (μ) for the distribution of six parameters is close to zero as the change in relative-rate-of-expansion resulting due to estimated location parameters is very small for the distances covered during constant-r segments. Moreover, the estimated scale parameters (σ) of $m_{[0-0.5]}$ and $m_{[0.5-1]}$ distributions are approximately twice the scale parameter of $m_{[0-1]}$ distribution. Similarly, the scale parameters of $c_{[0-0.5]} - r^*$ and $c_{[0.5-1]} - r^*$ distributions are approximately twice the scale parameters of $c_{[0-1]} - r^*$ distribution. Therefore, we represent the location parameters for all six distributions with the expected value zero and scale parameters of $c_{[0-1]} - r^*$, $c_{[0-0.5]} - r^*$, $c_{[0.5-1]} - r^*$, $m_{[0-1]}$, $m_{[0-0.5]}$, and $m_{[0.5-1]}$ distributions as σ_1, $2\sigma_1$, $2\sigma_1$, σ_2, $2\sigma_2$ and $2\sigma_2$, respectively (where $\sigma_1 = 0.53$ and $\sigma_2 = 4.22$). We use the represented distributions in the constant-r extraction algorithm as they are very close to the estimated ones (Figure S6).

Along with aforementioned six parameters, we define three other parameters to calculate mean acceleration in the full segment ($A_{[\text{mean},0-1]}$) and its two equal halves ($A_{[\text{mean},0-0.5]}$ and $A_{[\text{mean},0.5-1]}$), where subscripts $[\text{mean}, 0-1]$, $[\text{mean}, 0-5]$ and $[\text{mean}, 0.5-1]$ denote the mean of the acceleration computed for a full segment, first half and second half of the segment, respectively (see Materials and Methods for definition of A). As these mean acceleration values are almost always negative for the manually-identified 355 constant-r segments (Figure S6), we use these three mean acceleration parameters to identify the track segments in which a bumblebee decelerated during its landing manoeuvre.

S1.8.2. Algorithm for automatic extraction of segments with constant relative-rate-of-expansion

To automatically identify the segments of constant relative-rate-of-expansion in each landing track, we used the following algorithm:

1. Beginning with the first data point in each track, we looked at t_w time points ahead where $t_w \in \{15, 16, \ldots, 49, 50\}$ and it denotes the size of different time-windows (or segments). We chose the minimum limit for the time points (15 data points) close to the median of time points observed in 355 manually-identified constant-r segments (18 data points). The maximum limit for the time points (50 data points) is chosen as the number of data points in most manually-identified constant-r segments (353 out of 355) were below 50. Note that any long deceleration phase with more than 65 data points will be captured as two (or more) segments, but that does not affect the results observed in our study.
2. We select all those segments which satisfy the following constraints:

$$\begin{aligned} &|c_{[0-1]} - r^*| \le f\sigma_1 \text{ and } |c_{[0-0.5]} - r^*| \le 2f\sigma_1 \text{ and } |c_{[0.5-1]} - r^*| \le 2f\sigma_1 \text{ and} \\ &|m_{[0-1]}| \le f\sigma_2 \text{ and } |m_{[0-0.5]}| \le 2f\sigma_2 \text{ and } |m_{[0.5-1]}| \le 2f\sigma_2 \text{ and} \\ &A_{[\text{mean},0-1]} \le 0 \text{ and } A_{[\text{mean},0-0.5]} \le 0 \text{ and } A_{[\text{mean},0.5-1]} \le 0 \end{aligned} \tag{S5}$$

   where f is a factor that decides the threshold on the variation allowed around the mean for first six parameters (see Section S1.8.4 for details). The first three constraints limit the variation allowed, around the constant r regression, for intercepts of first-order linear regressions in an arbitrary full segment and its two equal halves. Similarly, the next three constraints limit the variation allowed around zero for slopes of first-order linear regressions in a full segment and its two equal halves. The last three constraints helps in determining the track segments in which a bumblebee decelerates during its landing manoeuvre.
3. We repeat steps 1 and 2 for all data points in the landing track. The resulting set of selected segments contains segments that satisfy the constraint mentioned in Step 2 and may have some data points in common with other segments. Therefore, from the resulting set, we further find a subset of non-overlapping segments based on root mean square error (RMSE) in relative-rate-of-expansion. For a segment containing n data points and estimated

set-point r^*, RMSE error is calculated as given by Equation S6.

$$r_{\mathrm{RMSE}} = \sqrt{\frac{\sum_{i=1}^{n}(r_i - r^*)^2}{n}} \tag{S6}$$

where r_i is the relative-rate-of-expansion at i-th point in a segment. After computing r_{RMSE} for all selected segments, the subset of non-overlapping segments is found by first choosing the segment with lowest r_{RMSE} and discarding all other segments with which it has data points in common. The segment with lowest r_{RMSE} in the remaining set of segments is then chosen and the segments in the remaining set it overlaps with are discarded. This process is followed until there are no segments left to choose. The set of chosen segments are then all non-overlapping and satisfy the constraints given by Equation S5. We use RMSE error for this selection process as it favours the track segments with higher number of data-points.

The resulting non-overlapping segments in a landing track are identified as the constant-r segments.

S1.8.3. Verification of results from automatic constant-r detection algorithm

To verify the results from constant-r detection algorithm, we compared the dependence of set-points of relative-rate-of-expansion (r^*) with distance from the platform (y^*) for smaller data-set (313 landing manoeuvres in which constant-r segments were manually identified) and complete data-set (4,672 landing manoeuvres for factor $f = 1$). We observed that r^* increased significantly as y^* decreased with slope (time-to-contact-rate) estimate from regression for smaller data-set ($\dot{\tau} = -0.72$) being similar to the average slope (time-to-contact-rate) estimate for complete data-set ($\dot{\tau} = -0.81$).

S1.8.4. Effect of factor f

Varying factor f has an effect similar to varying the number of standard deviations around the mean (e.g., $1-2-3$ standard deviations for $68\%-95\%-99.7\%$ empirical rule) of a normally distributed variable. Thus, increasing f leads to the detection of more false positives and fewer false negatives. Specifically, the factor f in Equation S5 determines following two aspects:

1. the threshold of the variation allowed around the mean for each parameter ($c_{[0-1]} - r^*$, $c_{[0-0.5]} - r^*$, $c_{[0.5-1]} - r^*$, $m_{[0-1]}$, $m_{[0-0.5]}$ and $m_{[0.5-1]}$) (Figure S5a)
2. the percentage of values of each parameter that lie within f scale-parameter band around the mean (Figure S5b)

Increase in f increases the threshold allowed in variation of r for a track segment to be identified as a constant-r segment, and hence, higher f can result in detection of new constant-r segments along with possible increase in the width of constant-r segments identified with lower f. However, increase in f beyond a certain value results in higher probability of detection of false positives without much increase in the true positives. We performed a sensitivity analysis by systematically varying f from $0.25 - 2.5$ and analyzing its effect on distribution of set-points of relative-rate-of-expansion (r^*) identified, r^* dynamics with distance to the platform (y^*) and effect of environmental conditions on this dynamics (Figure S5c,d). We observed that all of these results remain essentially unaltered in the tested wide-range of f.

S1.9. Calculation of relative approach speeds of the hybrid landing strategy

We tested how the here-described hybrid landing strategy compares to both the constant-r strategy and the constant-$\dot{\tau}$ strategy. For this, we calculated for each set of two consecutive constant-r segments, the hybrid-to-constant-r speed ratio and the hybrid-to-constant-$\dot{\tau}$ speed ratio as U_H/U_r and $U_H/U_{\dot{\tau}}$, respectively. Here, U_H is the average flight speed during the set of two consecutive constant-r segments, defined as $U_H = \Delta y_2/\Delta t_2$, where Δy_2 and Δt_2 are the distance travelled and flight duration, respectively (Figure 4a in the main text). U_r is the equivalent flight speed if the bumblebee would have used the constant-r strategy and continued to fly at its first set-point (r_1^*), and is defined as $U_r = 2/(r_1^*(y_{start} + y_{end}))$, where y_{start} and y_{end} are the distances from the platform at the start and end of the flight section. $U_{\dot{\tau}}$ is the equivalent speed if the bumblebee would have used the constant-$\dot{\tau}$ strategy to fly continuously at the average time-to-contact-rate observed in our data-set ($\dot{\tau} = -0.87$), with an initial approach speed equal to that at the start of a flight section. The resulting average speed $U_{\dot{\tau}}$ is then calculated as the average of approach velocities computed using Equation S8a. For this purpose, we used 1008 instead of 1015 landing manoeuvres with two constant-r segments because remaining seven landing manoeuvres corresponded to bumblebees flying away from the platforms in between the two consecutive constant-r segments.

S1.10. Governing equations for a constant time-to-contact-rate landing strategy

For an animal approaching a platform (Figure 1a), at time t, we denote its distance to the platform as $y(t)$, approach velocity as $V(t)$, relative-rate-of-expansion as $r(t)$, time-to-contact parameter as $\tau(t)$, time-to-contact-rate parameter as $\dot{\tau}(t)$ and following holds:

$$V(t) = -\frac{dy(t)}{dt},\ r(t) = \frac{1}{\tau(t)} = \frac{V(t)}{y(t)} \text{ and } \dot{\tau}(t) = \frac{d\tau(t)}{dt} \tag{S7}$$

The equations that govern dependence of state variables r and V on y for a constant $\dot{\tau}$ landing strategy are derived elsewhere Baird, Boeddeker, Ibbotson and Srinivasan (2013) and only final equations are depicted here (Equations S8).

$$V(t) = c_1\ y(t)^{\dot{\tau}+1} \tag{S8a}$$

$$r(t) = c_2\ y(t)^{\dot{\tau}} \tag{S8b}$$

where c_1 and c_2 are constants that depend on initial conditions of the state variables y, V and r.

S1.11. Parametrization of probability density functions used in this study

We use two probability density functions (pdf) in this study which are parametrized as follows:

1. Gamma distribution (*GammaDistribution* in MATLAB 2020a) - For a shape parameter a and scale parameter b, the pdf of the gamma distribution is

$$p(x \mid a, b) = \frac{1}{b^a \Gamma(a)} x^{a-1} e^{\frac{-x}{b}} \tag{S9}$$

   where $\Gamma(\cdot)$ is the Gamma function.

2. Generalized student's t-distribution (*tLocationScaleDistribution* in MATLAB 2020a) - For a location parameter μ, scale parameter σ and shape parameter ν, the pdf of generalized student's t-distribution is

$$p(x \mid \mu, \sigma, \nu) = \frac{\Gamma\left(\frac{\nu+1}{2}\right)}{\sigma\sqrt{\nu\pi}\,\Gamma\left(\frac{\nu}{2}\right)} \left[\frac{\nu + \left(\frac{x-\mu}{\sigma}\right)^2}{\nu}\right]^{-\left(\frac{\nu+1}{2}\right)} \tag{S10}$$

   where $\Gamma(\cdot)$ is the Gamma function.

References

Baird, E., Boeddeker, N., Ibbotson, M.R., Srinivasan, M.V., 2013. A universal strategy for visually guided landing. Proceedings of the National Academy of Sciences 110, 18686–18691. doi:10.1073/pnas.1314311110.

Chang, J.J., Crall, J.D., Combes, S.A., 2016. Wind alters landing dynamics in bumblebees. Journal of Experimental Biology 219, 2819–2822. doi:10.1242/jeb.137976.

Straw, A.D., Branson, K., Neumann, T.R., Dickinson, M.H., 2011. Multi-camera Real-time Three-dimensional Tracking of Multiple Flying Animals. Journal of The Royal Society Interface 8, 395–409. doi:10.1098/rsif.2010.0230.

Svoboda, T., Martinec, D., Pajdla, T., 2005. A convenient multicamera self-calibration for virtual environments. Presence 14, 407–422. doi:10.1162/105474605774785325.